Macroscale Electrostatic Rotating Machines and Drives: A Review and Multiplicative Gain Performance Strategy

Daniel C. Ludois, *Senior Member, IEEE*, Kevin J. Frankforter, *Member, IEEE*, Baoyun Ge, *Member, IEEE*, Aditya N. Ghule, *Member, IEEE*, Peter Killeen, *Student Member, IEEE*, and Ryan Knippel, *Member, IEEE*

***Abstract*— The development of electrostatic rotating machines for macroscale power conversion has been largely sidestepped, given the uncertainty of its capabilities and place in the technological hierarchy. This article reviews prior and present works in macroscale electrostatic rotating machinery and identifies the relevant machine types, their limitations, and strategies for performance improvement. The separately excited synchronous electrostatic machine presents the greatest opportunity for competitive macroscale category-two machinery, and a strategy of multiplicative gains is established. The strategy spans machine modeling, optimization, gap media (gases, liquids, and vacuum), gap maintenance, advanced manufacturing techniques, and power electronic drives/control. Ultimately, the product of innovation gains across all these areas reveals that macroscale electrostatic machinery is possible and potentially competitive with magnetic machinery for specific areas, including position and hold, low-speed direct drive, and high-voltage utility generation applications.**

***Index Terms*— Capacitance, electrostatic machines, synchronous machines, variable frequency drives.**

I. Introduction

In 1748, Benjamin Franklin constructed a device capable of converting static electricity into rotary motion, i.e., the first electric motor [1]. His accomplishment occurred 73 years before Michael Faraday's magnetic homopolar motor captured the world's imagination in 1821. Despite a lifetime head start, the electrostatic rotating machine was immediately eclipsed when its magnetic cousin emerged. In short, the underlying physics and available materials of the magnetic machine supported the more immediate practical investigation and use, whereas the opposite was true of the electrostatic machine. Nearly three centuries after Franklin's initial discovery, the means exist today to propel electrostatic machine performance to levels competitive with, or superior to, magnetic machines within a variety of niche applications.

This article examines "modern" efforts (mostly 1900 forward) in macroscale rotating electrostatic machines and frames progress through a multiphysics perspective spanning modeling, optimization, materials, manufacturing, power electronics, and controls. Ultimately, evidence of multiplicative gains is used to showcase the stratagems that are closing the orders of magnitude performance deficiencies between electrostatic and magnetic machines at the macroscale and is the primary contribution of this article. While electrostatic machines are ubiquitous at the microelectromechanical systems (MEMS) scale, they are not the focus of this article and will be discussed only when the overlap between these communities merits elucidation. Relevant macroscale rotating machine applications include power generation, high-voltage dc (HVdc), mobile robotics, industrial automation, and low-speed direct drive machines.

The sections of this article are structured as follows. Section II reviews electric forces, electrostatic machine types, and their historical development. Section III argues for the separately excited synchronous electrostatic machine (SEM) as an ongoing development platform and presents SEM modeling and optimization, establishing the vectors for multiplicative gains. The remaining sections examine each gain vector individually: Section IV: gap media; Section V: gap maintenance and manufacturing; and Section VI: power electronics and drive control. The state of the art for electrostatic machines, recommended focus areas for research, and future prospects is discussed in VII. Discussion is followed by the conclusions in Section VIII. Numerical performance metrics for all the machine references are available in Tables II–V in Appendix I.

II. Review of Electrostatic Rotating Machine Types and Magnetic Analogs

A. Brief Overview of Electromechanical Forces

Before delving into electrostatic machine types and how they may be improved, a brief review of electrical forces is useful. All forces of electrical origin are due to the Lorentz

Manuscript received April 10, 2020; revised July 22, 2020; accepted August 18, 2020. Date of publication September 10, 2020; date of current version February 3, 2022. This work was supported in part by the U.S. National Science Foundation CAREER under Award #1452230 and in part by the Gordon & Betty Moore Foundation Inventor Fellows Program under Grant #6880. Recommended for publication by Associate Editor Joseph O. Ojo. *(Corresponding author: Daniel C. Ludois.)*

Daniel C. Ludois is with the Department of Electrical and Computer Engineering, University of Wisconsin–Madison, Madison, WI 53706 USA, and also with C-Motive Technologies Inc., Madison, WI 53704 USA (e-mail: ludois@wisc.edu).

Kevin J. Frankforter and Peter Killeen are with the Department of Electrical and Computer Engineering, University of Wisconsin–Madison, Madison, WI 53706 USA.

Baoyun Ge, Aditya N. Ghule, and Ryan Knippel are with C-Motive Technologies Inc., Madison, WI 53704 USA.

Color versions of one or more of the figures in this article are available online at https://ieeexplore.ieee.org.

Digital Object Identifier 10.1109/JESTPE.2020.3023118

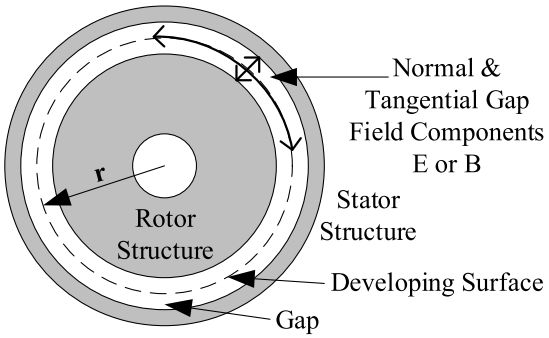

Fig. 1. Idealized radial flux rotating machine configuration.

force, as shown in (1) [2]. The Lorentz force describes the forces on the static and/or moving charge density ρ within a volume resulting from the presence of electric E or magnetic B fields. By applying Maxwell's equations to the source terms of (1), i.e., to eliminate the source terms by substitution, (2) is obtained

$$\boldsymbol{F} = \int_{x^3} (\boldsymbol{E} + \boldsymbol{v} \times \boldsymbol{B}) \rho dx^3 = \int_{x^3} (\rho \boldsymbol{E} + \boldsymbol{J} \times \boldsymbol{B}) dx^3 \quad (1)$$

$$\boldsymbol{F} = \int_{x^2} \boldsymbol{T} \cdot d\boldsymbol{x^2} - \varepsilon_r \varepsilon_0 \mu_r \mu_0 \frac{d}{dt} \int_{x^3} \boldsymbol{S} \cdot d\boldsymbol{x^3}. \quad (2)$$

Equation (2) contains two parts: the first is the Maxwell stress–energy tensor T, and the second is radiation pressure from Poynting's vector S. For low-frequency electromechanical systems, the radiation term is sufficiently small that it can be ignored, leaving only the stress tensor term. Elements of T have units of N/m^2 and are described by (3), where the subscripts i and j denote directional axes of the field components, e.g., $i = j$ (diagonals) – pressures and $i \neq j$ (off diagonals) – shears

$$T_{ij} \equiv \varepsilon_r \varepsilon_0 \left(E_i E_j - \frac{1}{2} \delta_{ij} E^2 \right) + \frac{1}{\mu_r \mu_0} \left(B_i B_j - \frac{1}{2} \delta_{ij} B^2 \right). \quad (3)$$

Electric machines derive torque, whether magnetic or electrostatic, from the off-diagonal shear terms of T acting on a developing surface at radius r. Whether electrostatic or magnetic, (3) shows that the components of T have the same functional form, which suggests that electrostatic machines can be largely described by magnetic analogs with some exceptions. These exceptions are notable and discussed first.

All rotating machinery can be generically described by the diagram shown in Fig. 1, where structures supporting current-carrying windings (magnetic) or capacitive electrodes (electrostatic) facilitate shear stress in the gap. However, some electrostatic machines can complicate matters by their mode of operation. Electrostatic machines fall into two categories: Category I: charge flow in the gap and Category II: no charge flow (ideally) in the gap. Category I machines rely on mobile charge in the gap (arcs, sparks, coronal partial discharge, friction, and so on) to facilitate their overall shear stress development. The first electrostatic machines discovered were this variety and include "friction," "influence," and "corona" machines. Category II machines do not have gap conduction and rely on the charge distributions confined to the stator and rotor surfaces resulting from the external connection or electric induction. Category II machines include "variable capacitance" (VC) (switched or synchronous), "commutated dc" and "ac synchronous" (separately excited or electret), "dielectric hysteresis," and "asynchronous induction." Of these, category II electrostatic machines have direct magnetic analogs, as shown in Table I, while category I machines do not since magnetic charge does not exist, and the currents are confined to discrete windings.

TABLE I
ELECTROSTATIC AND MAGNETIC MACHINE ANALOGS

Electrostatic Configuration	*Category*	*Direct Magnetic Analog*	*Magnetic*
Friction, Influence, Corona	I	No	----------
Variable Capacitance (switched or synchronous)	II	Yes	Switched or Synchronous Reluctance
Commutated DC and AC Synchronous (separately excited or electret)	II	Yes	DC and AC Synchronous (separately excited or Permanent magnet)
Dielectric Hysteresis	II	Yes	Magnetic Hysteresis
Asynchronous Induction	II	Yes	Asynchronous Induction

B. Category One Electrostatic Machines

Friction, influence, and corona machines, with pictorial examples shown in Fig. 2, will be discussed sparingly for brevity and are primarily included for the sake of reference. In the first two, the charge may be transferred by physical contact/rubbing (friction) or by natural imbalance that is amplified through a pumped action and picked up or deposited by combs (influence). Corona machines operate on the edge of breakdown (corona/partial discharge) and spray charge from the stator through the air gap to the rotor surface where it is repelled or attracted by the stator blades during rotation [3], [4]. These machines utilize dc sources and are self-commutating.

For the interested reader, Oleg Jefimenko's high-level and largely historical overview of electrostatic machines provides an excellent source of descriptions and references for further investigation into these machines [1]. Modern efforts exist in corona motors as they have provided the highest performance (power) in normal open-air atmospheric conditions at the macroscale compared with the other types of electrostatic machines but still lag magnetic machinery significantly in terms of both absolute power and power density. Detailed models of corona motor operation that accounts for the charge in the air gap and nonlinear corona effects are documented by Krein [5], [6]. Within the professional literature, macroscale

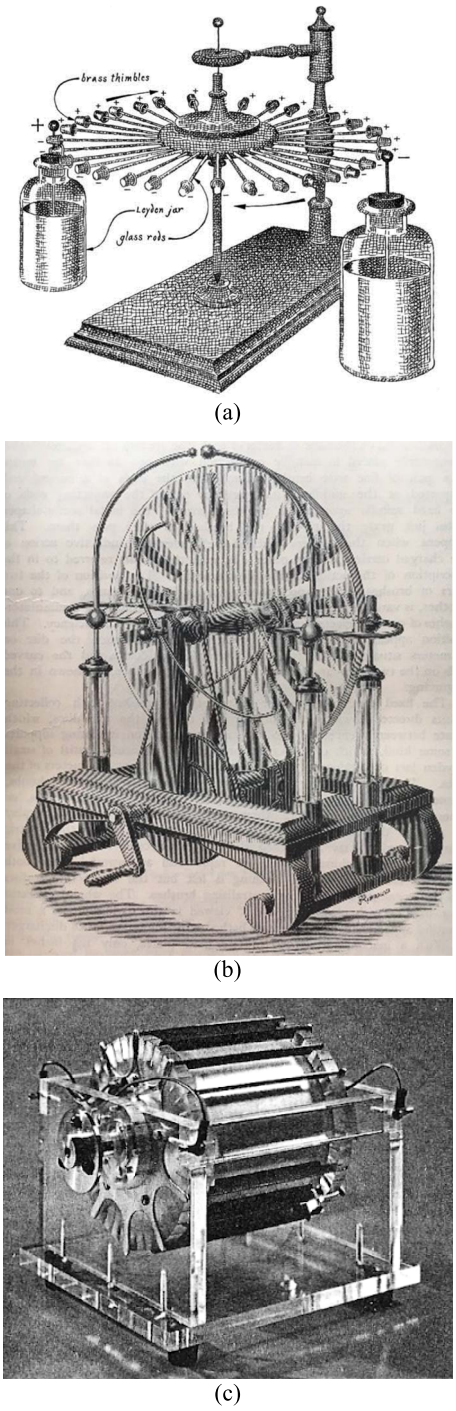

Fig. 2. (a) Franklin's electric wheel [8]. (b) Wimshurst's influence machine [9]. (c) Jefimenko's corona machine [1].

corona machines have demonstrated 10 s of mN·m of torque and 10 s of watts mechanical output with ∼15% efficiency [4]. Claims of 75 W and >50% efficiency have been made in the amateur scientist community [7].

C. Category Two Electrostatic Machines

Category II machines largely fall into operational modes that have direct magnetic analogs. Gap shear stress is facilitated by a variety of discrete stator and rotor configurations, with the

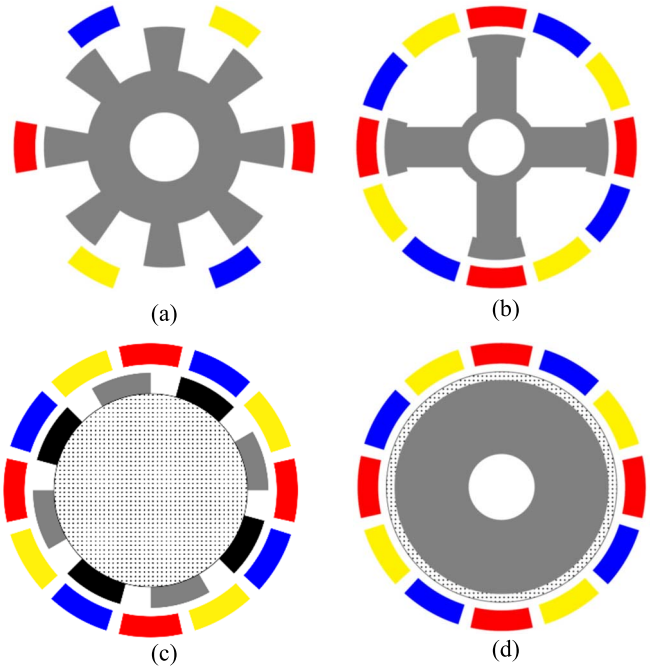

Fig. 3. Category II radial flux electrostatic machine conceptual diagrams of (a) stepped/switched variable capacitance, (b) synchronous variable capacitance (elastance), (c) separately excited synchronous, and (d) asynchronous induction [10], [11].

canonical example diagrams shown in Fig. 3 [10], [11]. All machine diagrams shown are polyphase (i.e., three-phase) ac configurations and generally conform to the well-established power flow rules of polyphase sinusoidal voltage and current waveforms, except for the pulsed waveforms of switched machines that are not a primary focus. The measured performance data for the historical machines presented are available in the Appendix.

First, the variable capacitance or elastance machines are shown in Fig. 3(a) and (b). Their magnetic analogs are switched and synchronous reluctance. The term "elastance" in capacitive systems is the dual of magnetic reluctance as coined by Heaviside [12] although it has not enjoyed widespread use in the power conversion community. The rotors of these machines are a single piece of conducting material that aligns and misaligns with different stator electrical axes during rotation, yielding spatial capacitive saliency. Torque is proportional to the applied stator voltage squared and the spatial derivative of capacitance as shown for switched (4) and sinusoidal machines (5)

$$T \propto \mathrm{V}_s^2 \frac{\mathrm{dc}}{\mathrm{d}\theta} - \text{switched} \tag{4}$$

$$T \propto V_s^2 \cos 2\gamma \ - \text{sinusoidal.} \tag{5}$$

These machines are distinguished by their voltage excitation, with step voltages applied for switched machine configurations [see Fig. 3(a)] and sinusoidal voltages for synchronous machines [see Fig. 3(b)]. Rotor position with respect to the stator must be known for proper commutation/control. Physical examples of macroscale VC machines

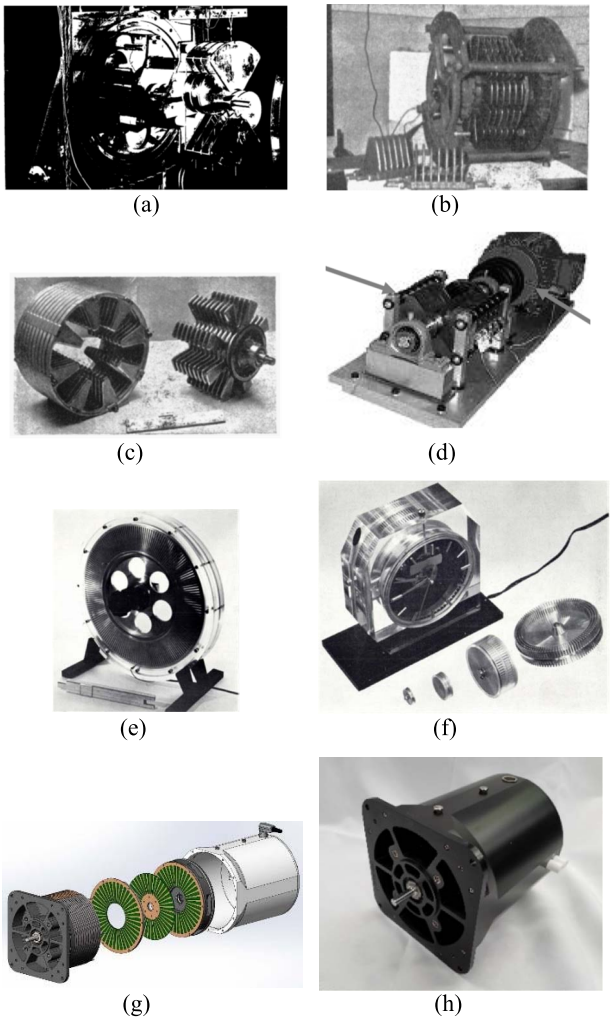

Fig. 4. VC machines. Vacuum insulated machines by (a) Trump [14], (b) and (c) Felici [15], and (d) O'donnell *et al*. [16]. (e) and (f) Open atmosphere machines by Bollée [17]. (g) and (h) Liquid-filled machine by CMT/ UW-Madison [13]. (b) and (c) 1953 IEEE. (d) 2009 IEEE. (e) and (f) 1969 IEEE. (g) and (h) 2017 IEEE.

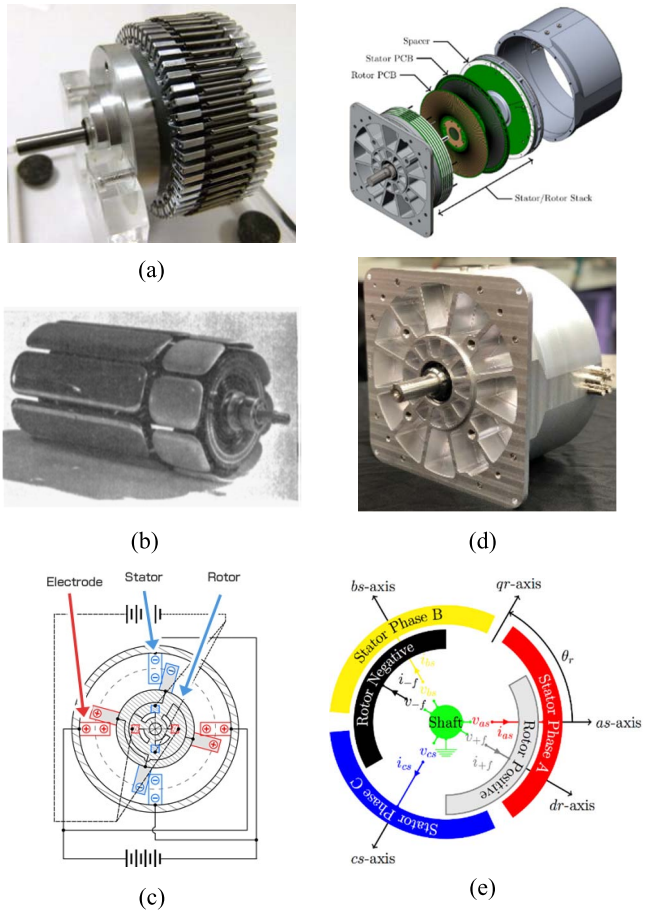

Fig. 5. Images of separately excited electrostatic synchronous machines. (a) Radial flux, vacuum insulated, commutated dc machine by Shinsei [19], [20]. (b) Brushessly excited dc machine rotor by Felici [15], [21], [22]. (c) Commutation diagram for a dc machine [19], [20]. (d) Exploded view and photograph of a liquid-filled ac separately excited synchronous machine by UW-Madison/CMT [23]. (e) Radial flux electrode diagram for machine in (d). (a) 2007 Shinsei. (b) 1953 IEEE. (d) and (e) 2019 IEEE.

are shown in Fig. 4, with a state-of-the-art example in Fig. 4(g) and (h) [13].

Second, separately excited synchronous machines are shown in Fig. 3(c). These machines have a three-phase array of stator electrodes and a two-phase rotor electrode array. The stator is excited with sinusoidal ac voltage, and the dc voltage is applied to the rotor. Torque is proportional to the product of stator voltage, rotor voltage, and the angle between them, as shown by the following equation:

$$T \propto V_s V_r \cos\gamma\,. \tag{6}$$

These machines need sliding electrical connections to the rotor for the rotor excitation voltage. The magnetic analog is the wound rotor synchronous machine. It should be noted that this machine could also be accomplished with permanently polarized electrets on the rotor in lieu of separate excitation, analogous to traditional permanent magnet machines. The dc electrostatic machines utilizing a brushed or semibrushless induction commutator also fall into this category since the stator and rotor electrodes merely swap physical locations (i.e., "inside-out") albeit with different terminal properties, analogous to magnetic machines [18].

The key power conversion element of these synchronous machines is that they produce a "back-current" rather than the back electromotive force (back EMF) of their magnetic analogs. The back current can also be referred to as a back magnetomotive force (back MMF), a terminology that maps familiar terms to these machines for the aide of drive analysis, but it should be noted that the machine does not use the back current to drive magnetic flux via Ampere's law for power conversion purposes. Physical examples of macroscale separately excited synchronous machines are shown in Fig. 5, with a state-of-the-art macroscale machine in Fig. 5(d) [23].

Third, asynchronous induction machines are shown in Fig. 3(d). The stator structure of this machine is identical to the ac synchronous machine and facilitates a traveling potential wave. The rotor structure is a continuous conducting substrate coated with a weakly conducting material, i.e., a "leaky" insulator. As the stator potential wave passes, it induces a

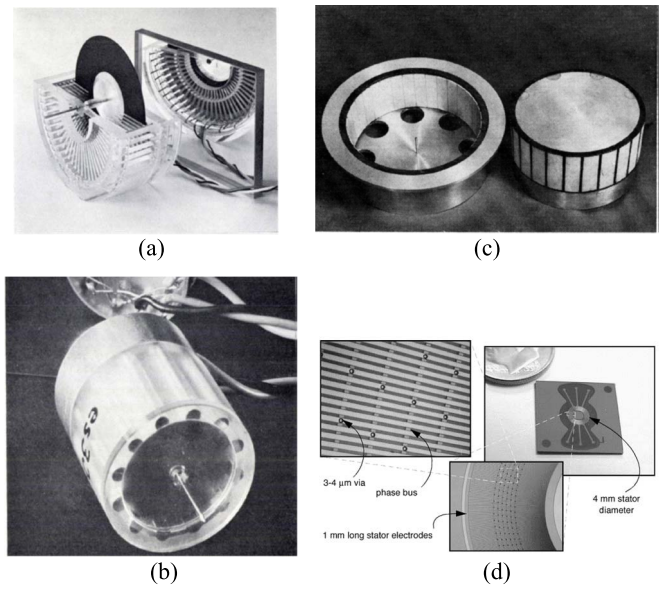

Fig. 6. Images of asynchronous induction and hysteresis electrostatic machines. (a) Bollée's axial flux asynchronous induction machine. (b) Radial flux induction machines [17]. (c) Vanslette's hysteresis machine [25]. (d) MIT asynchronous induction MEMS machine [24]. (a) and (b) 1969 IEEE. (c) 1965 IEEE. (d) 2005 IEEE.

charge distribution in the rotor that "slips" the stator field. Torque is proportional to the applied stator voltage squared, the rotor conductance, and the slip ratio, as shown by the following equation:

$$T \propto V_s^2 G_r \frac{1-s}{s}. \tag{7}$$

A slip-based machine is fundamentally limited in efficiency with an upper limit of (1-s), and typical slip values are in the single-digit percent range. The use of ferroelectric rotor materials can form synchronous hysteresis machines that start via asynchronous induction but are also limited in torque/efficiency capability given the area enclosed by the material's hysteresis curve. Despite these disadvantages, asynchronous machines have the advantage of self-starting from constant line frequencies, thereby circumventing difficulties of measuring the rotor position for commutation [24]. This advantage is particularly important for MEMS scales where additional shaft encoders and resolvers are not an option. Physical examples of macroscale asynchronous induction machines and hysteresis machines are shown in Fig. 6(a)–(c), with a state-of-the-art MEMS-scale machine in Fig. 6(d) [24].

D. Historical Development Evolution and Macroscale Limitations

VC machines first appeared in the 19th century and were constructed purely for research purposes by many scientists and engineers. These machines could provide high frequencies at high potential and were useful in a variety of physics experiments. Nikola Tesla remarked in 1891 that, while interesting from a research perspective, the constructed electrostatic machines were of no practical use compared with magnetics [26]. The first true attempt at a VC machine of industrial utility was pursued by Trump in 1933 [14] while studying under van de Graaff at MIT. In his thesis, Vacuum Electrostatic Engineering, he reported ten configurations of axial flux electrostatic machines working with ac or dc, ultimately prototyping a single-phase ac VC machine with an ultrahigh vacuum (UHV) as the essential insulating medium. Trump's VC machine, as shown in Fig. 4(a), was intended to demonstrate electrical generation directly at high-voltage transmission levels without the need for a step-up transformer. This machine could also serve as a high potential source for nuclear accelerators. Felici [15], [21], [22] followed suit with significantly improved VC machines, as shown in Fig. 4(b) and (c), and separately excited machines shown in Fig. 5(b) during 1940–1960, albeit with a focus on providing high-quality high-voltage power as a current source for nuclear experiments, vacuum tubes, and industrial electrostatic processes. Ultimately, the rise of semiconductor devices during this time diminished these pursuits in favor of solid-state high-voltage power conversion. Philp [27], [28] at General Electric Co. published a 9-MW paper design in 1977, which outlines the use of a VC machine with diodes as a charge pump for HVdc applications, potentially simplifying the overall HVdc architecture. Philp's approach was revamped and improved upon for offshore wind turbine farm concepts by O'Donnell *et al.* [16] in 2009 with supporting lab-scale experimental results. Shinsei Corporation showcased a 100-W separately excited dc electrostatic machine for operation in high-magnetic-field medical environments, but, ultimately, no product ever came to market [19]. To date, the authors are unaware of any successful commercial deployment of electrostatic rotating machines for the purpose of significant power conversion at the macroscale. The microscale, however, has enjoyed more success with asynchronous induction machines, the foundation of which was laid during the "space race."

Spacecraft system design during the 1960s sparked interest in electric machines that could operate in a vacuum without cooling, a natural fit for electrostatics [29]. Industrial experimental efforts at Philips and Northrop introduced serious work in asynchronous induction and hysteresis machines, respectively. Bollée's [18] team at Philips constructed three-phase induction machines shown in Fig. 6 (a) and (b) and could be used in low-power mechanisms when ran at line voltages (240 V, 50 Hz). These machines were also used to line start synchronous VC machines, such as Fig. 4(e). At Northrup, Vanslette [25] evolved the weakly conducting dielectric coating of the asynchronous machine to a ferroelectric one, yielding a self-starting hysteresis machine suitable for driving low torque mechanisms, as shown in Fig. 6(c). In parallel, but slightly later than these efforts, comprehensive analytical modeling of the electrostatic induction machine (and most other configurations) from a gap shear stress perspective was documented by Melcher [30] in his remarkable work *Continuum Electromechanics*. Others at the Jet Propulsion Laboratory and Stanford University followed Melcher's approach with experimental results as well [31]. Shortly after Melcher's work, Krein's thesis [6] developed a two-phase α–β lumped

element model of the induction machine with slip, mapping the operation into a steady-state understanding analogous to traditional induction machines. This modeling was pursued more recently by Santana *et al.* [32].

None of these rotating machines efforts were put to immediate practical use, but they helped set the stage for electrostatic rotating machines to enter the MEMS revolution of the late 1980s. The fabrication processes of the semiconductor industry created a means of etching microstructures on silicon and coating them with any number of thin materials. The windings-free, 2-D structure of electrostatic machines is a natural fit for this process. Scaling laws also favor electrostatics in MEMS, where reasonable supply voltages ($\leq$100 V) facilitate appreciable shear stress given the small physical dimensions and improvements in electric breakdown strength [33]. Excellent examples of electrostatic induction micromotors were developed by Lang's team at MIT, where Melcher's models were paired with a scaling down of prior induction machine experimental work to reach speeds into the hundreds of thousands of RPM [24], [34]–[37].

An entire electrostatic rotating machine community has grown at the MEMS scale but not at the macroscale, which leaves the question of "why?" electrohydrodynamics (EHDs) among industrial electrostatic processes have seen the development and commercial use, but macroscale electrostatic rotating machines have made comparably little progress for two reasons.

1) Relatively low gap shear stress at atmospheric conditions combined with a lack of high-voltage control [38]. Equation (3) reveals just how significant this is. At 1.5 T, a field achievable with iron, the theoretical magnetic shear limit is 1.79 MPa or 260 psi. At 3 kV/mm with atmospheric conditions, the theoretical electric shear limit is 79.65 Pa or 0.012 psi, a $\sim$4 orders of magnitude deficiency for electrostatics compared with magnetics [39].
2) Magnetic machinery has steadily satisfied humanity's technological needs at almost every turn through evolving forms, i.e., historically, there has been a limited need for macroscale electrostatic rotating machines.

Historical and ongoing methods to circumvent the technical issues associated with macroscale electrostatics (#1) are covered in the remaining sections, but significant roadblocks lay ahead for magnetics (disrupting #2) in emerging applications, including industrial automation and mobile robotics (position and hold) and low-speed direct drive machines (hub motors, ship propulsion, wind or ocean wave generation, and so on). Magnetic machinery suffers significantly at low to zero speed at the rated torque because of conduction losses in the windings and pays an extreme volume and materials penalty for efficient operation, i.e., they get large and expensive quickly as speed drops [40]. Electrostatic rotating machines do not suffer from the conduction loss problems of magnetic machinery, as their torque is based on voltage, not continuous current flow [38]. Therefore, if the shear stress deficiency overcomes, electrostatics can help satisfy the growing emerging field of direct-drive low-speed applications with favorable scaling properties and loss management.

III. Separately Excited SEM: Argument in Favor, Shear Stress Modeling, and Multiplicative Gains

A. Argument for Separately Excited Synchronous Machines at the Macroscale

The selection of the category II electrostatic machine type is paramount given the four orders of magnitude deficiency in shear stress that must be recouped. From a torque density and efficiency perspective, it is prudent to compare the machines at hand and select a candidate that provides the best development platform. Recently, Lipo and Liu [41] Lipo *et al.* [42] did one such comparison, wherein the canonical magnetic machine topologies were analyzed based on torque production capability (accounting for machine type and losses) normalized to an "ideal" machine from Esson's rule [43]. Using these criteria, the rank of canonical magnetic machine types is given as follows:

1) rare-earth surface permanent magnet machine ($\tau = 1$);
2) rare-earth interior permanent magnet machine ($\tau = 0.9$);
3) salient-pole-wound field synchronous machine ($\tau = 0.83$);
4) round-rotor-wound field synchronous machine ($\tau = 0.707$);
5) induction machine ($\tau = 0.65$);
6) synchronous reluctance machine (0.6).

The analysis is based on terminal properties and high-level design via air-gap flux and surface current densities. This application of the Lorentz force cannot directly map as a starting point to electrostatics because the charge distribution is not readily known on the surface of a conductor in advance. However, the Maxwell stress tensor shows that the magnetic and electric terms are identical in form; thus, the same "air gap" conclusions map into the electrostatic domain with the exception of losses in the stator and rotor structures. What diminishes τ for the machines without permanent magnets is the rotor conduction losses, deriving rotor magnetization from the stator terminals, or both. Electrostatic synchronous machines do not exhibit any rotor conduction losses (ideally) but induction machines do (they operate via slip and, thus, require weakly conducting materials). In addition, the induction machine and VC synchronous machine derive their excitation entirely from the stator, thus paying torque density and control penalties. While the dual of permanent magnets exist in the electret, there is currently no "rare-earth" strength electret. In fact, electrets are orders of magnitude weaker than what separate excitation of the rotor can provide via direct connection to an external voltage source [44]–[46]. Extensive work in brushless excitation for magnetic systems should map to electrostatics albeit with accommodations for higher voltages, e.g., turns ratios or rotating voltage multipliers [47]. Furthermore, the surface electrodes in a separately excited SEM can be essentially near zero thickness, whereas finite thickness electrets could increase rotor volume at the macroscale. These qualitative arguments based on duality suggest that the separately excited SEM constitutes a near "ideal" electrostatic machine and holds the dual top rank spot of the ($\tau = 1$) rare-earth SPM machine. The remainder of this article will focus on the separately excited SEM as it has

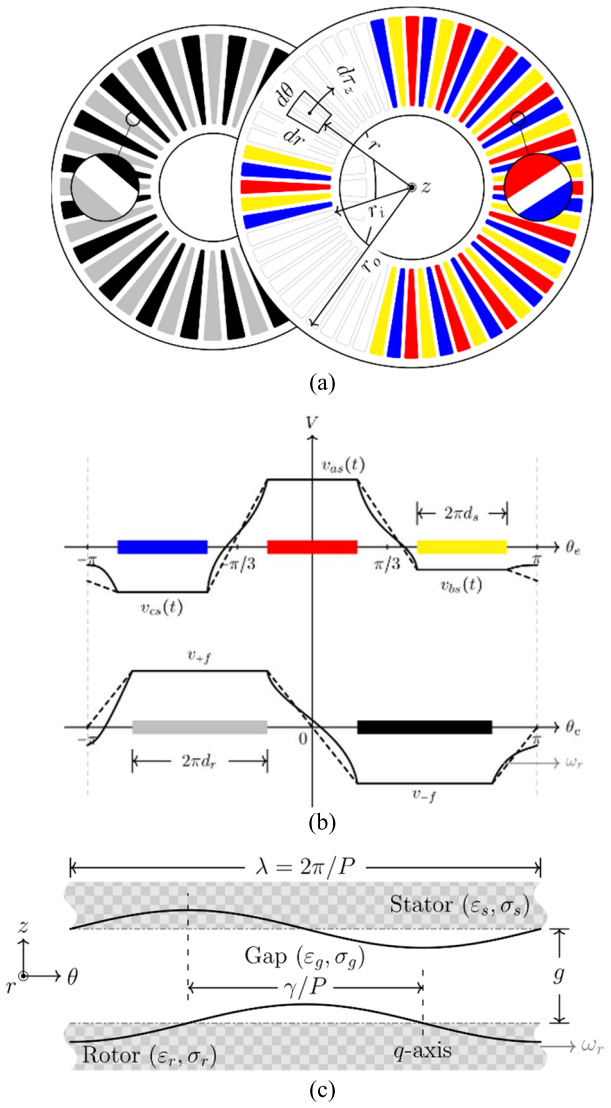

Fig. 7. Axial flux separately excited SEM configuration diagrams. (a) DC rotor-left, three-phase stator-right. (b) Radial profile view depicting discrete air gap potential waves. (c) Idealized sinusoidal potential version of (b) with parameters and dimensions identified for torque production. [23].

the broadest performance potential as a torque platform at the macroscale among category II electrostatic machines.

B. SEM Shear Stress Modeling and Multiplicative Gains

An axial-flux rotor-stator diagram of the separately excited SEM is pictured in Fig. 7(a) with a two-phase dc rotor field that faces a three-phase ac stator. These disks have P poles and are separated by a gap g that is filled with a medium of permittivity ε_g and conductivity σ_g. The potential waves that result from discrete electrodes are shown in Fig. 7(b). Melcher [30] derived the shear stress within the gap per assuming ideal sinusoidal potentials along with the parameters defined in Fig. 7(c).

Using the assumption of sinusoidal conditions, the torque per unit area at a given radius of an axial flux machine is given by (8), and the absolute torque is obtained by integrating over all the surfaces of the machine using (9)

$$\tau_z = -\frac{\varepsilon_g P^2}{2r \sinh\left(\frac{Pg}{r}\right)} V_s V_r \cos(\gamma) \tag{8}$$

$$T_{e,\max} = 2N \int_{r_i}^{r_o} \int_0^{2\pi} \tau_z|_{\gamma=\pi} \cdot r d\theta \cdot dr. \tag{9}$$

The discrete nature of electrodes' effect on the potential waves may be analyzed piecewise with the Fourier analysis to determine the fundamental spatial components that produce torque. This spatial harmonic analysis was done for separately excited SEM design in [10] and [23] and has been analyzed in both macroscale and MEMS induction motors in [6], [24], [34], and [48]. Equations (8) and (9), when paired with spatial harmonic analysis, yield accurate results as verified by experimental measurements in [10] and [23].

These equations serve to showcase the handles available for machine design from a torque production perspective. The handles appear as individual quantities (e.g., gap permittivity ε_g or the number of rotor disks N) and as parametric ratios (e.g., Pg/r); thus, any given design space should be swept by conventional optimization techniques. A complete discussion of tradeoffs among the variables within (8) and (9) that incorporates the discrete electrodes of Fig. 7(b) is presented in [10] and [23]; however, more straightforward design insights, regardless of detailed analysis, include the following.

1) The number of rotors should be large, i.e., to increase the area per unit volume.
2) The radius should be large, e.g., a "pancake" form factor is attractive.
3) The gap should be tiny compared with the radius, i.e., to increase the mutual capacitive coupling.
4) The gap medium should possess high-permittivity, high-breakdown strength material if possible.
5) The stator and rotor potential waves should be large in amplitude with $\gamma = 0$.

With respect to implementation, these items generally oppose one another. For example, items 1 and 2 together make item 3 mechanically difficult, i.e., gap maintenance. Item 4 suggests altering the machine's gap medium to be an environment other than normal atmospheric conditions, complicating the mechanical design further and potentially introducing unconventional materials. Item 5 requires the manipulation of high voltage with control for both spatial and temporal variability, i.e., a variable frequency drive with the field (charge)-oriented control.

Innovations in given Sections IV–VI constitute the multiplicative gain thrusts that support macroscale machine progress, regardless of machine configuration. Optimization of a specific design is where the details of a given configuration become important, e.g., a separately excited SEM versus a VC machine. In the case of the separately excited SEM, optimizing the torque of the machine given a set of constraints is straightforward by standard analytical methods since the analytical model described by (8) and (9) is very accurate. The five design guidelines outlined earlier fulfill much of the design optimization since the torque is mostly monotonically dependent on these parameters/thrusts.

At present, the construction materials of electrostatic rotating machines also tend to be more linear than their magnetic counterparts; thus, saturation limitations on analytical methods are not as prevalent. This may change as ferroelectric materials enter designs. Switched elastance or VC machines generally seek to maximize $dC/d\theta$, which is akin to shear stress but it is in a discrete form via a terminal perspective. The efforts to maximize $dC/d\theta$ by sweeping parametric ratios are documented in [49] and [50], and the efforts in topological optimization have emerged more recently [51]. The thickness of the electrodes is of great importance in torque production as well because of the dielectric stress on the ambient medium. In VC machines, Felici [15] determined the optimum ratio between the gap distance and the electrode thickness as 1:1 or 1:2 to assure uniform dielectric stress on the ambient medium.

IV. Gap Media in Electrostatic Machines

Modifying the gap medium to facilitate higher electric shear stress is usually the first step to improve electrostatic machine performance. According to (3), (8), and (9), this is achievable through raising the electric field breakdown strength, the relative permittivity, or both [39]. Raising the breakdown strength can be achieved in one of three ways: high-pressure gas (HPG), UHV, and dielectric liquids. The relative permittivity of HPG and UHV is unity because the space between molecules dominates, or in other words, the absence of matter defines free space. Dielectric liquids exhibit relative permittivity but also introduce losses through electrical conductivity and kinematic viscosity.

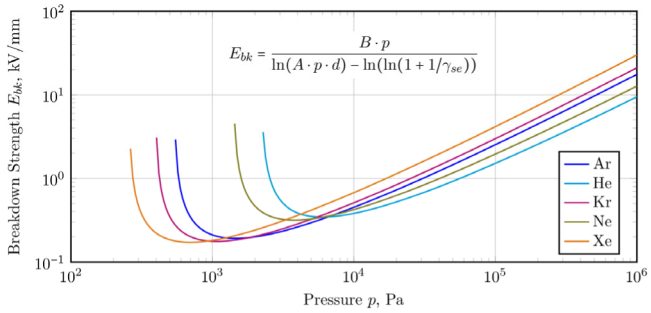

(a)

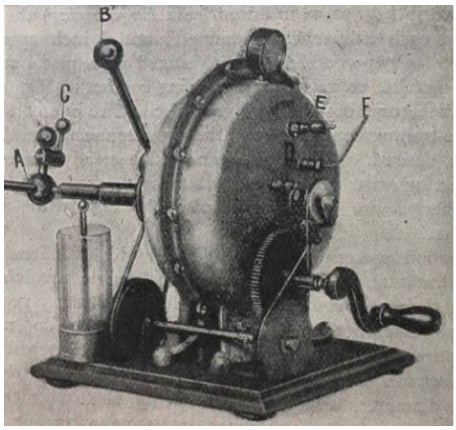

(b)

Fig. 8. (a) Paschen's curve obtained for argon, helium, krypton, neon, and xenon. Parameters A and B are taken from [52], d is the separation distance between electrodes, and γ_{se} is the secondary electron emission coefficient at the cathode and is set to 0.01. (b) Tudsbury influence machine circa 1900 [9].

A. HPG and UHV Gap Media

HPG and UHV exhibit breakdown characteristics that are largely described by Pashcen's curve, with example breakdown versus pressure curves for various gases in Fig. 8(a) [52]. The curves show that conditions approaching vacuum or high pressure increase breakdown strength. An early example, perhaps the first, to take advantage of these properties for electrostatic rotating machinery was done by Tudsbury in 1900 [9]. The Tudsbury influence machine was built inside of a pressure vessel, as shown in Fig. 8(b). Air was pumped through a drying mechanism into the machine at a pressure of 60 PSI, increasing the output spark length (and, thus, voltage) from 2.5 to 8 in. Tudsbury remarked on the need to repressurize the machine every few days due to the leaky seals where the shaft exited the vessel. Nevertheless, this set the stage for the next generation of machines utilizing pressure vessels some decades later.

The pursuit of high voltage for nuclear accelerators in the first half of the twentieth century saw this pressure vessel concept greatly improved at both ends of Paschen's curve [53]–[55]. UHV methods favored electrostatic machinery where the shaft exits the machine vessel to a mechanical prime mover in normal atmospheric conditions. The absolute pressure across the shaft seal in the UHV case is 1 atm (15 PSI). For HPG configurations, the mechanical prime mover for the machine (generator) could be located inside the pressure vessel, and no shaft seal is needed, thereby affording 10 s of atm (hundreds of PSI) more easily. HPG is a difficult choice for electrostatic machines that intend to drive mechanical loads outside the pressure vessel, given the pressure differential imposed on the seal. UHV approaches for rotating machines were implemented successfully at ∼100 kV by Trump [14] and Felici [15] with HPG implementations, achieving 250 kV also by Felici [22] and discussed by Vanslette [25]. The most recent UHV incarnation was exhibited by Shinsei [19] with a 100-kV, 10k-rpm, 100-W machine [19]. Ultimately, both UHV and HPG do increase shear, but the lack of relative permittivity means the applied voltage must still be very high (hundreds of kV) to facilitate adequate shear stress at the macroscale [39].

B. Dielectric Liquid Media

Dielectric liquids offer Maxwell stress beyond UHV and HPG through the use of dielectric permittivity in addition to breakdown strength. The upper bound of this stress is determined by the electrical breakdown strength of the liquid and its conduction loss. Depending on the kinetic nature of the electrostatic system, the viscosity of the fluid may also be a critical concern. Minimizing viscosity will obviously reduce any viscous losses seen by the system but further, by reducing viscous drag forces the speed range of the system will be extended, increasing its maximum power capability. Finally, dielectric fluids are often required to assist in the thermal management of a system, in addition to providing

their insulating and force-generating capabilities. Fluids with a high thermal capacity and thermal conductivity are beneficial, as is a low viscosity when performing convective heat transfer operations, e.g., to get heat out of the machine or process. Liquids exhibit excellent performance at atmospheric pressure, allowing the pressure gradient across the vessel housing to approach zero and minimizing the shaft seal complexity. Manipulating the pressure of the liquid media (and, thus, Paschen's curve) has been proposed [56], but the benefits of this additional complexity have not been quantified in the literature. Liquids are also incompressible, and therefore, a liquid-filled machine may be suitable for high-pressure environments where compressive forces are a concern (e.g., undersea).

With the aforementioned material properties in mind, the chemistry of various liquid systems immediately forces one to focus on certain classes of materials while excluding others. It is desirable for the fluid to exhibit a large permittivity, which is a consequence of the electric dipole moment of its constituent molecules, but the conductivity of most of the most polar fluids significantly limits their application. The foremost example of this is H_2O. Due, in part, to its high polarity, the relative dielectric constant of water is in excess of 80, on the larger range of values demonstrated by liquids [57]. However, even when rigorously purified and all external contaminants are removed, water will spontaneously autoionize, releasing the mobile charge carriers OH^- and H^+ (or more precisely, H_3O^+). Because of its propensity to autoionize, the minimum conductivity of liquid water is approximately 5.5×10^{-6} S/m, while fluids with conductivities on the order of 10^{-10} S/m or less are preferred to limit electrical losses in macroscale applications, e.g., to take advantage of near-zero conduction loss. Similarly, there are several classes of compounds that demonstrate high dielectric constants but are also limited by their propensity to autoionize, such as alcohols and carboxylic acids. Essentially, any compound with appreciable acidity will suffer from this effect, limiting design choices to primarily aprotic solvents.

Further limiting the available choices for dielectric fluids is the need for a high degree of chemical stability, mechanical compatibility, low toxicity, low flammability, and a minimal environmental impact. Dielectric fluids must be resistant to degradation, with oxidation and hydrolysis reactions being a primary concern due to oxygen and water, which will be absorbed by most liquids when in contact with the atmosphere. The electrostatic system can be closed to the atmosphere and/or blanketed with inert gas, but this limits the application of liquids with high volatility due to excessive evaporation rates in open systems and excessive pressures during temperature swings. Another avenue for the degradation of the fluid arises when it is exposed to high strength electric fields. Breakdown of the constituent solvent molecules of the dielectric liquid, or rather any less stable molecule present as an impurity in the liquid, is often accompanied by the generation of free radicals [58]. Free radicals are powerful chemical reactants, which will further degrade the dielectric fluid, and can potentially generate new charge carriers, detrimentally increasing its conductivity. Generated free radicals can be quenched by additives, such as butylated hydroxytoluene, to prevent further degradation of the dielectric fluid, an approach that is common in the oils used for the electric transformer industry [59].

Regardless of their internal diversity, each of these categories has various strengths and weaknesses compared with the categories. Mineral oils contain mixtures of longer chain alkanes but will generally be limited by their viscosity. Shorter chain alkanes, such as hexanes, have very low viscosity but will be much more volatile and significantly flammable. Conversely, silicone oils are significantly nonflammable and can be tailored to have very low viscosity while retaining low volatility. A weakness of silicone oil is its hygroscopic nature due to its siloxane backbone (-Si-O-Si-O-). As such, it will readily absorb moisture from the atmosphere to the detriment of conductivity and electrical breakdown strength. Esters are somewhat more polar than mineral and silicone oils and, therefore, provide a slightly greater dielectric constant. Esters can be derived from biorenewable sources with a minimal carbon footprint and are generally nontoxic. A primary drawback of esters is their susceptibility to hydrolysis due to water, and the degradation products of which (alcohols and carboxylic acids) can increase the acidity of the dielectric fluid and generate charge carriers. Finally, the halocarbons used for dielectric fluids are generally alkanes in which a number of hydrogen atoms are substituted with halogen atoms (fluorine, chlorine, and so on). This can impart polarity upon the molecule and significantly improve its chemical and thermal stability. Unfortunately, halocarbons tend to be expensive; there are relevant concerns related to the toxicity of the compounds and their synthetic precursors; and a large number of halocarbons have a significant global warming potential (GWP) and/or ozone depletion potential (ODP) values, which prevents their usage.

These various dielectric liquids have been employed by various researchers over the years for electrostatic machines, but the published reports generally focus on aspects of the machines other than the liquid itself. The first reports of using an oil in the stator–rotor gap of an electrostatic machine was in the 19th century for corona machines [1], but Vanslette [22] and Felici [25] explored the topic more thoroughly during the 1960s for category two machines. Vanslette employed an unspecified "silicone-nitrile" fluid that was verified to enhance the magnitude of the displacement field by a factor of 20. It is significant to note, however, that the high viscosity of the liquid prevented any testing at synchronous speed (1500 RPM). Felici explored, unsuccessfully, the use of nitrobenzene as limitations on contaminant induced conductivity and the material's general toxicity prevented further development [22]. Gradually, efforts in the understanding of space charge [60] and conduction modes of dielectric liquids subjected to high field strength [61] improved liquids. In 1995 and 1997, Niino *et al.* [62], [63] described a small linear electrostatic machine in which silicone oil ($\varepsilon_g/\varepsilon_0 = 2.2$) and a fluorocarbon (a 3-M Fluorinert compound, $\varepsilon_g/\varepsilon_0 = 1.9$) were used to prevent dielectric breakdown and briefly compared. Unfortunately, there are scant details about the fluids used other than their relative permittivity and results demonstrating their force production.

More recently, there have been several articles published from Ludois and colleagues on advanced electrostatic rotary machines in various configurations. Their initial work extensively utilized the fluorocarbon Vertrel XF [13], [38], [39], [64]–[66] produced by Chemours (previously DuPont) due to its high relative permittivity (7.1) and low viscosity (0.67 cP); however, in later publications, a different fluorocarbon, Vertrel Sinera [49], [67], was used due to its lower volatility and increased boiling point, despite having a lower relative permittivity (5.5). This trend has continued to their most recent reports; in [23], an unspecified dielectric fluid ("HT101") was utilized with a relative dielectric constant of 3.8, despite having the same reported electric field breakdown strength (20 kV/mm) as the previous Vertrel fluids. In [68], the ester isoamyl isovalerate was used as the base solvent in a dielectric nanoparticle suspension, where a dielectric constant of 4.0 and the conductivity on the order of 10^{-9} S/m were reported. A fluid-filled induction-type electrostatic machine filled with the fluorocarbon Novec 7100 ($\varepsilon_g/\varepsilon_0 = 7.4$) was reported on by Dadkhah *et al.* [69]. Other approaches have been proposed that examine the use of organic carbonates [70]–[72], such as propylene or ethylene carbonate, as these have excellent dielectric constants [57]. However, the family of carbonates suffers from numerous chemical issues regarding conductivity management already described, and no successful machine has been published.

In addition to reports detailing linear and rotary electrostatic machines in more traditional form factors, there is also a blooming field of electrostatic actuators (or dielectric fluid transducers) for soft robotics applications and energy harvesting. These devices also use dielectric liquids for enhanced Maxwell stress. First described in [73], the Keplinger Research Group has published several reports on what they term a hydraulically amplified self-healing electrostatic (HASEL) actuator, in which the attractive force developed by flexible electrodes printed on an elastomeric pouch containing a dielectric liquid is used to control a hydraulic functionality based on the shape of the pouch. These reports [74]–[80] have exclusively utilized Cargill FR3 natural ester-based transformer oil as their dielectric liquid, which has a relative permittivity of 3.2 [81]. An independent report on HASEL actuators produced by Park and Cha [82] utilized Mictrans A, an uninhibited mineral oil intended for use with transformers. Lin and Liu [83] reported on a similar soft electrostatic actuator but utilized the ester isopropyl myristate ($\varepsilon_g/\varepsilon_0 = 3.1$) as their dielectric fluid. Finally, the Fontana Research Group has published a report on a novel fluid transducer in [84], in which the silicone oil Xiameter PMX-200 50CS was utilized, and later described a HASEL actuator utilizing MIDEL 7131, a synthetic ester-based transformer oil ($\varepsilon_g/\varepsilon_0 = 3.2$), in [85]. VC energy harvesters [86], [87] and brushless rotary power transfer approaches [88] have demonstrated the use of ionic conducting electrolytes to exploit the double-layer capacitor effect, but this is an entirely different electrostatic liquid mechanism than previously described since charge carriers are in the gap (Category I).

Within all these pursuits, the current published state of the art for measured Maxwell stress in liquids is 2 PSI (13.8 kPa), a 300x improvement over the air, but it only closes two of the four orders of shear stress deficiency compared with magnetics [39]. Synthesis of new dielectric liquids for increased Maxwell stress is an area ripe for research, but other multiplicative gain thrusts must be employed in parallel to close the performance gap.

V. Gap Maintenance and Manufacturing

Electrostatic machines can afford disruptive manufacturing approaches compared with their magnetic counterparts given their unique features. They do not need to be made of iron, copper, or rare-earths and are potentially lower materials' cost and more sustainable when considering the long-term availability of elements [13], [89]. The foremost enabling feature is that electric flux lines terminate on charge and do not need to form a closed-loop path, i.e., electrostatic machines "require" surfaces, not volume, to accrue electric charge. Magnetic machines by contrast require the flux lines to cross the air gap, flow-through "back iron," and cross the air gap again to their source making these machines inherently more 3-D (although it should be stated that the presence of iron in this flux loop is equivalent to filling the electrostatic machine gap with a dielectric). The large 2-D attributes of electrostatics afford three unique manufacturing design properties: 1) the stators and rotors may be cascaded one after the other within a volume; 2) thin conductors only need to reside on the surfaces of the rotor and stator, and 3) the stator and rotor substrates may be insulators [38]. These properties enable electrostatic rotating machines to be extended/stacked to the maximum extent possible within a given volume, thereby increasing the area for electric shear to act upon.

Cascading gaps within the machine volume has been practiced since the days of influence machines [1], and Trump [14] and Felici [15] (shown in Fig. 4) pursued axial flux cascaded gaps extensively for macroscale VC machines. Individual "plates" with vanes cut from metal sheets were cascaded along a shaft, much like RF tuning capacitors. Axial flux cascaded disks have been shown to provide the highest surface area per unit volume in rotating capacitor applications [90], but not without difficulties. Felici, in particular, lamented the difficulty of maintaining a consistent axial gap along with the cascaded stack for the machine in Fig. 4(c), wherein machining tolerances of the 1/100th mm were not sufficient to maintain the gap parallelism during operation when projected to the end of the stack. This limited the operating voltage, significantly reducing system performance. The pressure terms of the Maxwell stress tensor (3) act to collapse the gap and can deform the disks/plates, reducing gap distance or even crash the rotors, especially in axial flux configurations [91]. Radial flux gaps more easily manage this compared with their axial counterparts because the Maxwell pressures cancel radially for concentric cylinders. Modern advancements in magnetic axial flux machines and other mechanical devices led to bearing offerings, such as "deep groove" ball bearings and "angular contact" bearings that can manage radial and axial shaft forces simultaneously [92], [93]. The electrostatic machines in [13] and [23] have deployed these shaft bearings

in the "end bells" to maintain 12 0.8-mm axial gaps between six rotors and seven stators. This number of rotors, stators, and gaps constitutes an order of magnitude higher surface area per unit volume over magnetic machinery. This leap in surface area is another multiplicative gain, and the efforts in this regard are numerically recorded in the Appendix. Reducing the gap further at the macroscale beyond the capabilities of current ball bearing technology requires more exotic approaches.

1) *Mechanical Contact Type Bearings Inside the Gap:* Dadhaka *et al.* [69] suspended 55-μm glass beads in 3M Novek 7100 to maintain the axial gap between machine components. The addition of Novek 7100, a dielectric liquid, not only served to bolster the electrical performance of the machine but also added lubricity between the contacting components, reducing the effects of mechanical wear. Others have proposed the use of discrete ball bearings inside the gap as well [98].
2) *Aerostatic & Hydrostatic Bearings:* These bearings rely upon an externally pressurized source of dielectric fluid to generate a repulsive force between the rotor and stator sections of the machine, counteracting the Maxwell pressure. The noncontacting nature of these bearings is associated with extremely low running friction, and hence low drag torque, but comes at the cost of being reliant upon an external fluid pump and ancillary plumbing. Nevertheless, hydrostatic bearings have seen use in several successful electrostatic machine designs. In [94], air pressure exerted through holes in the stator periphery was used to float the rotor above the stator with an axial spacing of 350 μm at a maximum rotor speed of 250 rpm, as shown in Fig. 9(a). Because of the low parasitic friction inherent in their design, hydrostatic bearings (both journal and thrust) were chosen to maintain the 4-μm gap in the ultrahigh-speed MEMS electrostatic induction machine designed and presented in [35], [99], and [100] with the design and engineering of the bearing discussed in [100].
3) *Aerodynamic & Hydrodynamic Bearings:* Gap maintenance following this regime is reliant on the relative motion of stationary and rotary components to sweep fluid into the gap to create pressure rather than rely on an external source. This can be accomplished principally upon the shape and surface features of the facing surfaces. The approach has seen success in rotating capacitive power transfer systems [95], [101]–[104] with particularly high surface area per unit volume achieved by spiral groove bearing geometries [95], [102]. Spiral grooves are reliefs in the surface that traps fluid to build pressure as it is channeled into the gap. The depth of the bearing groove, the density and viscosity of the working fluid, and the operational speed of the machine determine the performance. Full theoretical models of hydrodynamic bearings may be found in [105]. This was first achieved in the MEMS VC machine shown in Fig. 9(c) [96], where a spiral groove thrust bearing was etched into the nontorque producing region of the rotor. This concept was taken a step further in [106] and [107] where the dielectric liquid serves to increase shear and provide gap maintenance simultaneously. The demonstration was shown in [91] and [97], where the poles of the ES machine were formed as herringbone groove features shown in Fig. 9(d) and (e), allowing them to be dual purposed as both the torque and thrust producing mechanisms in the machine. While effective as gap maintenance, it required a catch or touchdown bearing to be used while the machine operated below

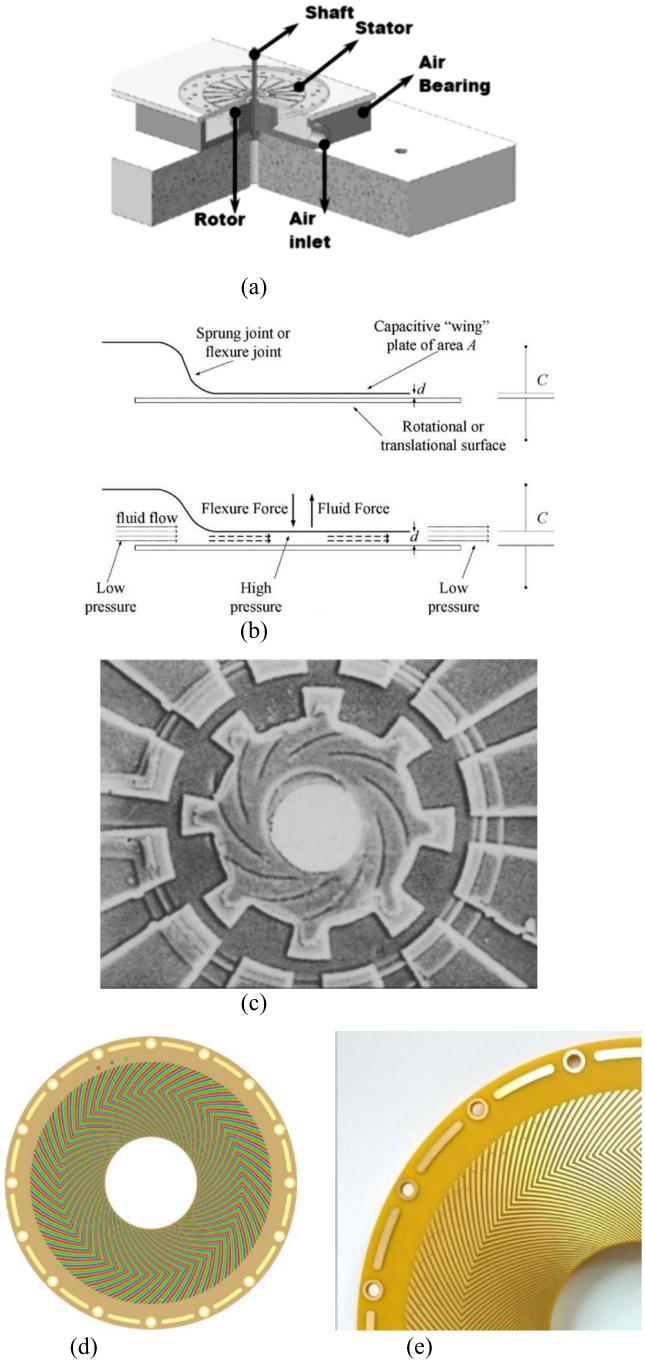

Fig. 9. Gap maintenance approaches. (a) Aerostatic bearing arrangement [94]. (b) Hydrodynamic foil bearing [95]. (c) Spiral groove thrust bearing in MEMS VC machine rotor [96]. (d) Three-phase electrodes as spiral grooves in PCB stator. (e) Experimental implementation of (d) [97]. (a) 2007 IEEE. (b) 2014 IEEE. (c) 1993 IEEE. (d) and (e) 2019 IEEE.

the critical speed of the bearing. Alternative versions of the hydrodynamic gap maintenance are foil or "wing" bearings on flexures shown in Fig. 9(b), which has been proposed or employed in [95], [106], and [108].

4) *Electrostatic Bearings:* These bearings use the Maxwell pressure in the gap to manipulate the distance directly. Discrete surfaces of an electrostatic apparatus are dedicated to levitation/suspension by means of VC/variable elastance forces in conjunction with a controller. This approach has been employed at the MEMS scale in rotating machines in [109]–[111] and at the macroscale for suspension of processes, e.g., hard drives and silicon wafer processing [112]–[114]. The approach is in its infancy for application to macroscale power conversion but interest in gap maintenance for flywheels and machines is emerging [115], [116].

Early macroscale machines were constructed of discrete metal surfaces or plates, as already mentioned, but advanced manufacturing creates opportunities for weight savings and lower materials cost. The first demonstration of a plastic construction electrostatic machine was done by Bollée [17], where the stators and rotors of a radial flux synchronous VC machine were machined from methacrylate and then coated with aluminum by vapor deposition, as shown in Fig. 10(a). Krein [6] demonstrated a variety of discrete plastic constructions as well, but used adhered foil [6]. Cascaded radial gaps were extremely impractical to construct at the time given the complexity of the machining. Practical cascaded radial gaps have been implemented using a dowel pin insert approach, where multiple rows of concentric pressed pins are embedded in rotors and stators and connections made in the substrate [19], [38], [65]. An example dc machine is pictured in Fig. 5(a). In recent years, though, pin construction has been displaced by 3-D printing, where stators and rotors of nearly any shape can be constructed through additive processes, thus negating the difficulties of conventional machining [49], [117]. A single-phase radial flux switched VC that was 3-D-printed in plastic and coated with 0.001" layer of nickel is shown in Fig. 10(b) [49]. Ultimately, though, the axial flux machine will be the dominant configuration at the macroscale given its larger surface area per unit volume. This advantage is further supported for machines <500-mm diameter as the established, low-cost manufacturing process of printed circuit boards (PCBs) readily supports that size range. The axial flux cascaded gap switched VC machine in Fig. 4(g) uses a PCB construction, as shown in Fig. 10(c) and (d) with the PCB structural data available in [91] and [97]. Perhaps, the most useful aspect of the PCB approach, though, is that it naturally supports multipotential surfaces with ease while 3-D printing and discrete metal plates do not (presently). The three-phase ac PCB stator and the two-phase dc PCB rotor of the separately excited SEM in Figs. 5(d) and 7 are shown in Fig. 10(e) and (f), respectively.

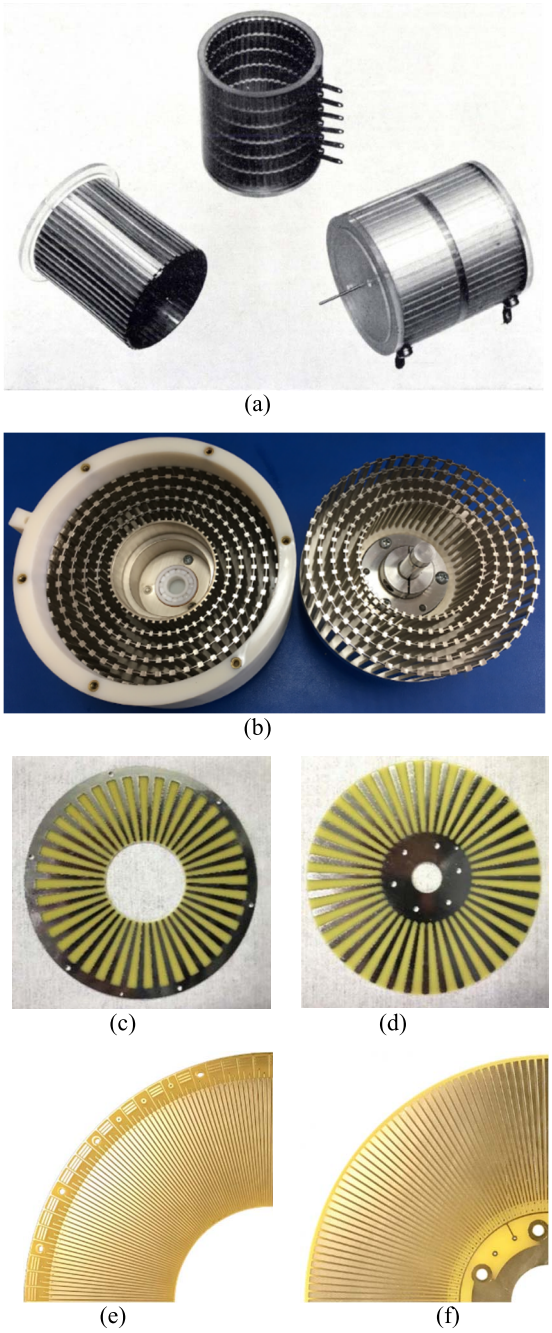

Fig. 10. Electrostatic machines using insulating substrates with surface conductors. (a) Machined plastic with vapor deposited aluminum [17]. (b) 3-D printed plastic with nickel plating for a multigap, radial flux VC machine [49]. PCB construction for VC machine (c) stator and (d) rotor [13] and for separately excited SEM (e) stator and (f) rotor [23]. (a) 1969 IEEE. (b) 2016 IEEE. (c) and (d) 2017 IEEE.

VI. Recent Efforts in Circuit Modeling, Power Electronics, and Drive Controls

Generalized circuit models for drives were developed for three-phase electrostatic machines, covering both synchronous and asynchronous types to understand torque production, as well as form a basis for vector control [23]. Unlike magnetic machines where the conduction paths are confined within windings, the leakage current field in the machine is colocated with the electrostatic field. Thus, between any pair of terminals in Fig. 11(a), there are capacitances and conductances in parallel, which adds one more layer of complexity to this highly coupled system. If the machine is filled with a dielectric fluid, then gap conduction loss is blended into the *dq*-axis

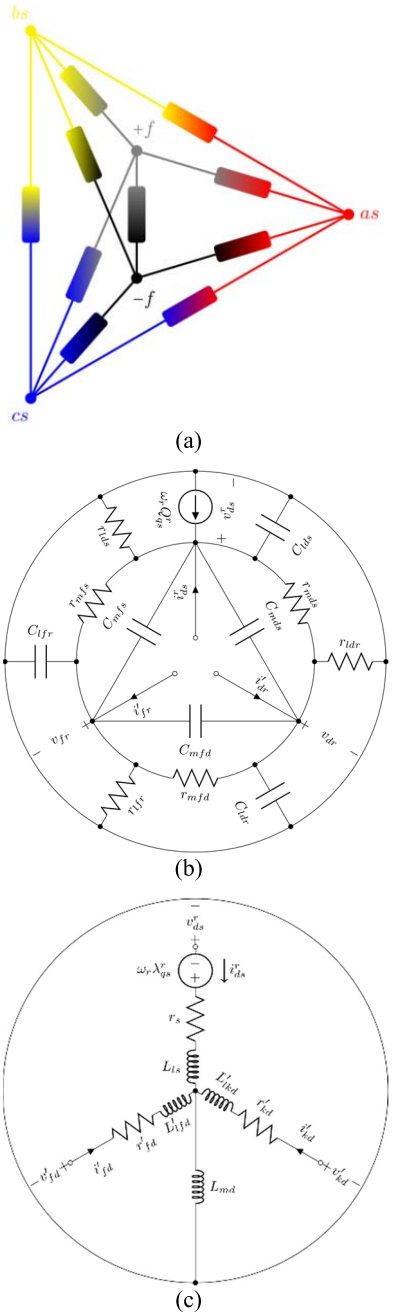

Fig. 11. Generalized equivalent circuit modeling for the separately excited synchronous machine with damper surfaces [23]. (a) Terminal model with capacitance/conductance coupling. (b) d-axis model of electrostatic machines. (c) d-axis model of magnetic machines for duality reference. (a)–(c) 2019 IEEE.

model. The resultant d-axis circuit is shown in Fig. 11(b) with the canonical magnetic salient pole synchronous machine with dampers included for reference Fig. 11(c). Although the circuit may be drawn directly via the electric–magnetic duality, the model fidelity comes from its preservation of the electric field's unipolar nature, which is reflected in the dc-biased capacitance distribution of the circuit. As a result, the key terminal capacitances were pinpointed for torque optimization, and the field torque is deployed to increase the torque density by a factor of five [23]. This terminal behavior observation also supports the earlier argument that the separately excited SEM poses a higher torque performance among the category two electrostatic machines. Another interesting result is the existence of resistive saliency that inversely tracks the capacitive saliency; this was experimentally confirmed in [13].

The generalized torque equation of the separately excited SEM with damper surfaces is shown in the form of modern drives in (10), including saliency torque (elastance), field torque (separate field excitation or electrets), and induction torque (slip). Field-oriented control (FOC) in magnetic machinery can map into electrostatics but with an emphasis on the charge, rather than flux. In a separately excited SEM, charge-oriented control refers to the placement of the rotor excitation on the d-axis, whose derivative is the back current (MMF) on the q-axis [118]. Alignment of the applied stator voltage with the d- and q-axes

$$T_e = \frac{3P}{2}\left\{\underbrace{(C_{ds}-C_{qs})v_{qs}^r v_{ds}^r}_{\text{elastance torque}} - \underbrace{C_{mfs}v_{qs}^r v_{fr}}_{\text{field torque}} - \underbrace{C_{mds}v_{qs}^r v_{rd} + C_{mqs}v_{ds}^r v_{rq}}_{\text{induction torque}}\right\} \quad (10)$$

as indicated by (10) and the phasor diagram in Fig. 12(a), determines the resultant torque. If the SEM possesses saliency, then proper orientation can result in torque stemming from both field and elastance components though control. The maximum torque per volt condition angle is shown in Fig. 12(b). The induction torque component of (10) only applies to SEMs with dampers driven from constant frequency mains. An SEM paired with a variable frequency drive is always self-synchronized and does not require dampers. However, regulating the voltage on the different axes with variable frequency introduces the need for power electronics and control methods.

Power Electronics & Drive Controls: The emergence of drive technology constitutes the final multiplicative gain to enable electrostatic machines. Historically, the majority of electrostatic machine research is from a machine perspective, with attention to drive electronics and control as an afterthought. MEMS machinery can afford this luxury since the small power levels of the machine, relatively low operating voltage afforded by microdimensions, and high fundamental frequency naturally lend the system to analog amplifier solutions. Constant- or near-constant-speed applications can utilize step-up transformers to connect the machine to a low voltage supply but are application-specific, e.g., self-starting slip-based induction machines [24], [37], [62], [119] and utility-level voltage synchronous VC machines [14]. Also, transformer approaches are not suitable for general-purpose variable frequency drive use due to core saturation at low frequencies and operational resonances with the capacitive machine [11]. An interesting approach to eliminate the transformer and simultaneously provide a dc output in HVdc generator applications is Philp's configuration, as shown in Fig. 13 [28]. This simple power electronics approach is achieved with passive

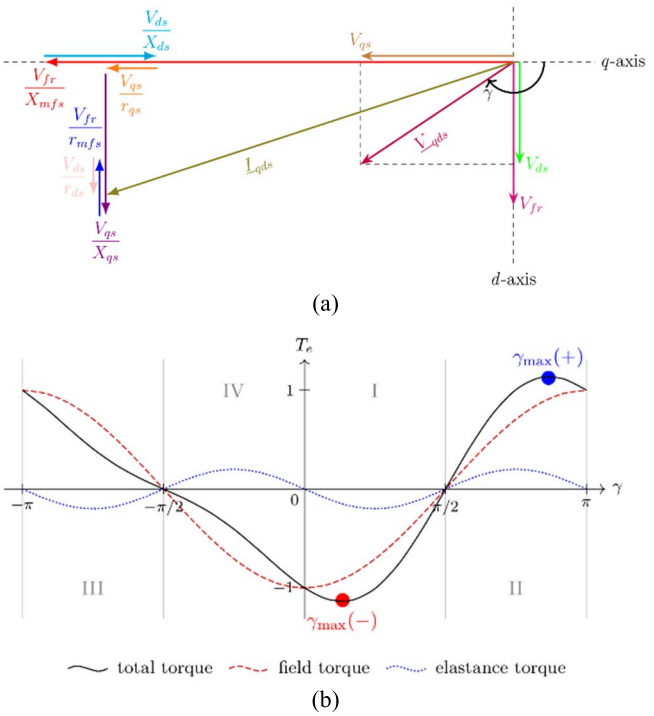

Fig. 12. (a) Separately excited SEM phasor diagram and (b) max torque angle with field and saliency components [23].

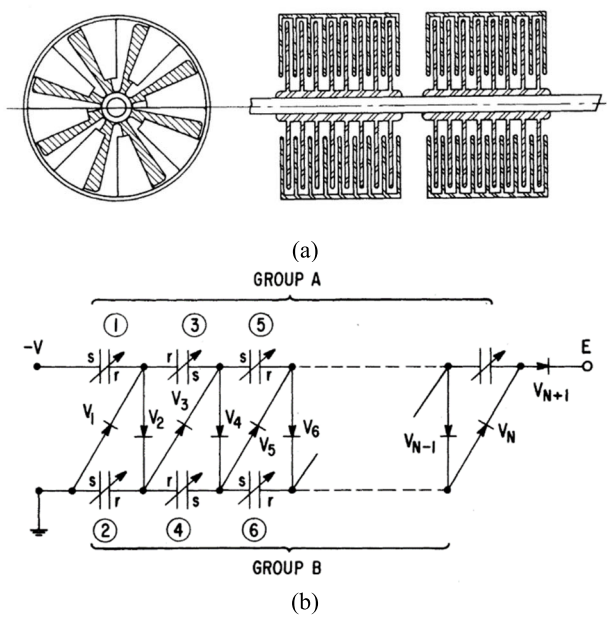

Fig. 13. (a) Philp's switched VC machine for HVdc and (b) machine diode connections for charge ladder or multiplier [28]. (a) and (b) 1977 IEEE.

diode commutation and is readily scalable to transmission line voltages, but its usefulness is very niche.

Macroscale electrostatic drives intended for servo or propulsion purposes are almost unheard of and have only recently emerged alongside competitive machinery. Shinsei offered a separately excited dc machine with a brushed commutator [19], [20], simplifying the drive electronics to a 100-kV dc power supply, but no mechanical or electrical closed-loop control in this approach was presented. The dc power supplies of very high voltages can be made with ease using lower voltage parts, e.g., the Cockcroft–Walton voltage multipliers, but their single quadrant operation prohibits them from supporting an ac machine with bidirectional power flow. Recently, a 5-kVrms current-source inverter (CSI) ac drive was developed using series-connected IGBT switches [120] for the separately excited SEM in [23]. The CSI naturally "boosts" voltage, which is attractive for systems with lower voltage input power sources, and it is directly compatible with electrostatic machinery's innate *RC* terminal characteristics [11]. Another advantage of the CSI is the ability to source ampere–seconds (charge) to manipulate terminal voltage, a natural fit for the field (charge)-oriented control [121].

Although the voltage-source inverter (VSI) is a more familiar topology in motor drives, it requires an intermediate inductive filter for connection to an electrostatic machine. A VSI controller would require an inner current loop for the inductors to provide charge-oriented control. Complex vector voltage regulators, paired with a CSI and charge orientation through encoder feedback, have been used for torque modulation in separately excited SEMs in [11] and [120]. The basic drive configuration is shown in Fig. 14(a), and it demonstrated servo level performance torque steps under variable frequency (speed) conditions, as shown in Fig. 14(b). An ongoing challenge of SEM drives is high fundamental electrical frequencies and spatial feedback resolution, even at low speeds, due to high pole count (P $\sim$ 100). This property leads to switching loss dominance in drive design and expensive position sensors. Tremendous progress has been made in sensorless (self-sensing) control of motor drives [122], with high-frequency signal injection and back-MMF (current) tracking approaches recently demonstrated in electrostatic machines to eliminate the need for position feedback sensors [11], [123].

The primary hardware challenge presented by macroscale electrostatic drive development is the lack of commercial off-the-shelf (COTS) semiconductor switch offerings with low-current (<5 A) and medium-voltage ($\sim$10 kV) ratings. For example, the drive shown in Fig. 14 requires devices capable of at least 10-kV blocking (7-kV peak line–line plus margin) with 1-A current rating. Multilevel VSIs would reduce the voltage requirements for each switch but introduce additional control complexity and cost [124], [125]. Surveying the semiconductors available for medium-voltage applications reveals general target power levels greater than 1 MW with current ratings greater than 100 A. These devices are not well-suited for low power (<100 kW). Emerging 10-kV silicon carbide (SiC) metal–oxide field-effect transistors (MOSFETs) with a $\sim$10–20-A current rating per chip would be a suitable candidate [126], [127], but the devices are not widely available, and most studies have focused on multichip power modules targeting high-power applications [128]–[130]. The alternative to a monolithic semiconductor switch is a series connection of lower voltage devices. In [120], four series-connected 3.6-kV silicon IGBTs were utilized per switch. However, this implementation requires individual medium-voltage isolated gate drivers for each

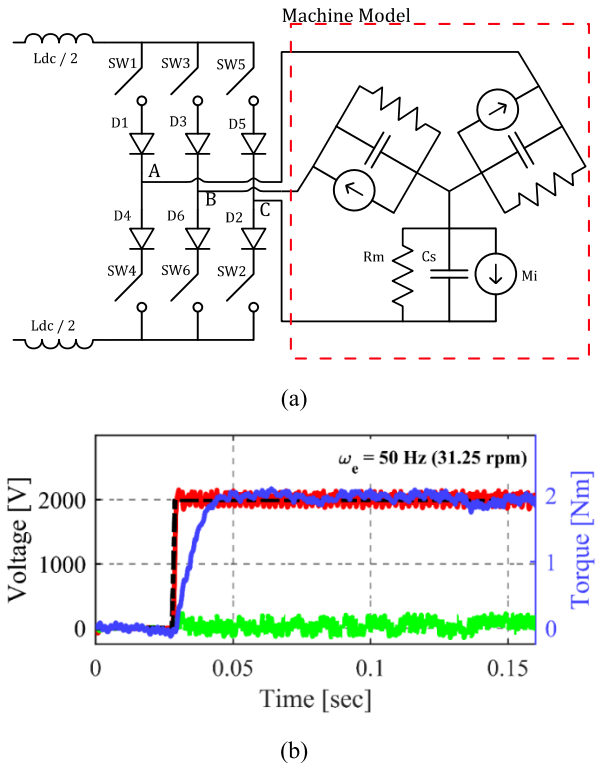

Fig. 14. CSI variable frequency drive implementation. (a) Topology diagram and (b) torque step of the machine at 50-Hz operating point [120]. Commands: $\mathbf{V_{qs}}*$ or $\mathbf{T}*$, Measurements: $\mathbf{V_{qs}}$, $\mathbf{V_{ds}}$, and $\mathbf{T}$. All in the synchronous reference frame. (a) and (b) 2020 IEEE.

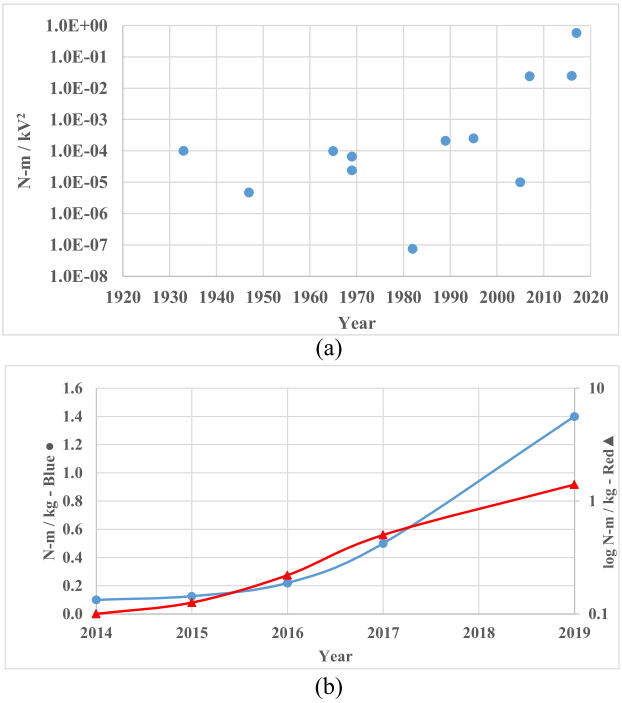

Fig. 15. Plots of the measured macroscale electrostatic rotating machine metrics. (a) Table II torque per kV^2 versus time. (b) Specific torque density versus time in linear and logarithmic scale [13], [23], [49].

device resulting in 24 large and expensive fiber-optically isolated gate drivers. While this maintained the simple control of a two-level CSI, the reduced implementation cost and size were lost. In [131], a normally-on JFET supercascode was developed for use in electrostatic CSI drives. The supercascode reduces the gate-drive requirement to six for a two-level drive, as is the standard for most drive topologies. Using a model for the supercascode from [131], Killeen and Ludois [132] compared the VSI and CSI topologies application spaces and concluded that the CSI topology is well suited for general-purpose variable-speed-drive applications, while the VSI is better suited for low-speed position and hold applications. This conclusion was further extended in [133] where a differential inverter is proposed to minimize loss for the position and hold applications while eliminating isolated gate drivers and other components for minimal drive volume.

VII. Discussion

Historically, electrostatic rotating machines have not been torque competitive with their magnetic counterparts, but this is changing due to the multiplicative gain design approach. In fact, Tables II and III show that electrostatic machines using the multiplicative gain approach have matched some of their COTS air-cooled magnetic counterparts in torque at the fractional horsepower level, with superior conduction loss characteristics at low speeds and stall. Examination of the torque production equations for the separately excited synchronous machine reveals the specific handles that can be manipulated as multiplicative gains, and these were identified as innovations spanning modeling, optimization, gap media, gap maintenance, advanced manufacturing, and power electronic drives. The product sum of incremental progressions across multiple handles can grow quickly, advancing electrostatic machine torque performance by order of magnitude beyond prior work. This is evident in Table II that tabulates the numerical data on available electrostatic machines with published results measured under the rated conditions. The machines with the highest absolute torque, torque per volt squared, and torque density use several multiplicative gains in concert, as suggested here.

Prior to recent times, rigorous multiplicative gain approaches were not deployed in macroscale electrostatic machines, as shown by plotting torque per kV^2 versus time data (from Table II) in Fig. 15(a). Similarly, Fig. 15(b) reveals the rapid progress in specific torque density in recent years as well [13], [23], [49]. As a whole, Fig. 15 suggests that, while many innovations occurred in the last century, net progress only results when innovations are merged in concert. While still emerging, favorable torque/loss characteristics, paired with ongoing drive development (see Table IV), may lead SEMs to be servos for robots, industrial automation, or flight surfaces. High-performance control methodologies for these machines have been established, but further development in power electronic hardware will be required to bring them into commercial use. Ultimately, higher power levels and continuous motoring operation will require further development among the multiplicative gain vectors.

Active material torque densities of 1.4 N·m/kg (0.76 N·m/kg total materials) were demonstrated in [23] with a liquid of

TABLE II
KEY METRICS AND MEASUREMENTS OF ROTATING ELECTROSTATIC MACHINES IN THE LITERATURE

Research Work in	Insulation Medium	Cascaded Gap	Adv. Manuf.	Power, W	Speed, rpm	Maximum Torque, N-m	Voltage, kV	Torque per Volt^2, N-m/kV^2	Type†	Scale‡
MIT (1933) [14]	UHV	Yes	No	5.5E+1	3.6E3	1.5E-1	7.3E+1	2.7E-5	VC	L
Grenoble (1947) [15]	HPG	Yes	No	5.0E+2	7.5E2	6.4E+0	2.5E+2	1.0E-4	VC	L
Northrop (1965) [25]	HPG	No	No	1.0E-2	1.5E3	7.5E-5	4.0E+0	4.7E-6	Hyst	L
Philips (1969) [17]	Air	Yes	No	1.0E-4	2.0E2	4.8E-6	2.2E-1	9.9E-5	VC	L
Philips (1969) [17]	Air	Yes	No	2.0E-4	6.0E2	3.2E-6	2.2E-1	6.6E-5	Indu	L
UIUC (1982) [6]	Air	No	No	2.0E-1	5.4E2	3.5E-3	1.2E+1	2.4E-5	Coro	L
MIT (1989) [34]	Air	No	MEMS	7.9E-7	1.0E4	7.5E-10	1.0E-1	7.5E-8	Indu	S
RIKEN (1995) [62]	Air	No	MEMS	3.6E-3	2.0E2	6.9E-4	1.8E+0	2.1E-4	VC	S
MIT (2005) [24]	Air	No	MEMS	5.8E-2	2.7E5	2.0E-6	9.0E-2	2.5E-4	Indu	S
Shinsei (2007) [20]	UHV	Yes	No	1.0E+2	1.0E4	1.0E-1	1.0E+2	1.0E-5	DC	L
UW-Madison (2016) [49]	Liquid	Yes	3D Print	2.0E+1	5.0E2	1.2E+0	7.0E+0	2.4E-2	Swit	L
C-Motive (2017) [13]	Liquid	Yes	PCB	3.0E+1	5.0E2	2.0E+0	9.0E+0	2.5E-2	Swit	L
UW-Madison & C-Motive (2019) [23]	Liquid	Yes	PCB	4.9E+2	5.0E2	9.3E+0	4.0E+0	5.8E-1	SEM	L

† VC—Variable Capacitance Machine, Hyst—Hysteresis Machine, Indu—Induction Machine, Coro—Corona Machine, DC—DC Machine, SEM—Separately Excited Machine. ‡ L—Macroscale, S—MEMS Scale.

TABLE III
COMPARISON OF FRACTIONAL HP SEM MACHINE MEASUREMENTS WITH THE SELECTED MAGNETIC MACHINES

Machine Model	Volume [L]	Weight [kg]	Torque [N-m]	Stall Loss [W]	Torque Density*	
					Volumetric [N-m/L]	Gravimetric [N-m/kg]
Bodine 34R6BFPP [1]	1.36	4.10	0.84	51.5	0.62	0.20
Leeson ZSP6-0602 [1]	2.73	7.71	1.37	---	0.50	0.18
Rel Tork 2-124SR-24 [2]	2.25	9.10	3.56	53.0	1.58	0.39
BLWS235D-160V-3k [3]	0.25	1.25	0.50	12.7	2.00	0.40
EMJ-04APB22 [3]	0.35	2.51	1.27	3.70	3.63	0.51
UW-Madison & C-Motive Prototype [4] [23]	5.20	12.2	9.35	1.27	1.79 (2.65)	0.76 (1.4)

[1] magnetic induction machine [2] magnetic switched reluctance machine
[3] permanent magnet machine [4] electrostatic synchronous machine
* all aspects of machine package, not just active components, e.g. case, etc. () - active components only

TABLE IV
OVERVIEW OF PRIOR ELECTROSTATIC MACHINE POWER SUPPLIES/DRIVE CONTROL IMPLEMENTATION

Research Work	**Type**	**Drive / Supply**	**Vpeak [kV]**	**Multi-phase**	**Variable Speed**	**Position Based Drive Output**
MIT (1933) [14]	VC	HV Transformer	100	No	No	No
Philips (1969) [17]	VC	LV Mains	0.31	Yes	No	No
U. of Tokyo (2011) [119]	VC	HV Transformers	0.9	Yes	Yes	No
MIT (2000) [99]	Ind	Linear Amp	0.11	Yes	Yes	No
MIT (2004) [37]	Ind	Multilevel VSI / Transformer	0.30	Yes	Yes	No
Shinsei (2007) [19]	DC	DC supply	100	NA	Yes	Commutator
UW-Madison (2016) [49]	VC	Linear Amp	10	No	Yes	Yes
C-Motive (2016) [13]	VC	Linear Amp	10	No	Yes	Yes
UW-Madison (2019) [23]	SEM	Linear Amp	10	Yes	Yes	Yes
UW-Madison (2019) [120]	SEM	CSI	7	Yes	Yes	Yes, servo

$\varepsilon_g = 3.8$ and a gap distance of 0.8 mm. Continued improvement in the synthesis of insulating dielectric liquids with enhanced relative permittivity (e.g., $\varepsilon_g \geq 10$) should enable existing electrostatic prototypes to reach active torque densities ≥ 4 N·m/kg (at $\varepsilon_g = 10$) with no cooling system needed. Such machines could be competitive with or superior to liquid-cooled permanent magnetic machines in low-speed direct drive applications. Furthermore, Table V reveals that the gap

TABLE V
COMPILATION OF GAP MAINTENANCE METRICS AND APPROACHES IN ROTATING CAPACITIVE MACHINERY

Institute, [Source]	Dielectric Gap [m]	Capacitive Radius [m]	Aspect Ratio	Normalized by [1]	Flux Direction	Bearing Type
UW-Madison (2019) [91], [97]	5.72×10^{-5}	8.50×10^{-2}	1490	1	Axial	Hydrodynamic, Aerostatic
Taribat Modares Univ., Ulsan Univ., Arak Univ. Sultan Qaboos Univ. (2015) [69]	5.00×10^{-5}	4.75×10^{-2}	950	0.637	Axial	Rigid
MIT (2001) [35]	4.00×10^{-6}	1.90×10^{-3}	475	0.319	Axial	Aerostatic
MIT (2000) [99]	4.00×10^{-6}	1.90×10^{-3}	475	0.319	Axial	Aerostatic
Jet Prop. Lab, Stanford U. (1971) [31]	6.53×10^{-4}	3.00×10^{-1}	459	0.308	Radial	Rigid
UW-Madison (2018) [102]	1.15×10^{-5}	4.70×10^{-2}	409	0.274	Axial	Hydrodynamic
UW-Madison (2019) [23]	7.62×10^{-4}	1.10×10^{-1}	144	0.097	Axial	Rigid
Univ. Pavita, Salford Univ. (2007) [134]	2.00×10^{-4}	2.84×10^{-2}	142	0.095	Radial	Rigid
Taribat Modares Univ. (2007) [94]	3.50×10^{-6}	1.30×10^{-2}	37.1	0.025	Axial	Aerostatic
UIUC (1982) [6]	4.00×10^{-3}	7.50×10^{-2}	18.8	0.013	Radial	Rigid
MIT (1933) [14]	1.00×10^{-2}	1.71×10^{-1}	17.1	0.011	Axial	Rigid

maintenance gain has not been fully utilized, as aspect ratios of an order of magnitude beyond [23] have been achieved. While it is unlikely that a 10x improvement in gap maintenance can be achieved for a multi-rotor–stator system, reducing the thickness of the PCBs and the gap by 30% each (for the same voltage) would enable another factor of $\sim$2, yielding $>$ 8 N·m/kg (at $\varepsilon_g = 10$). It is clear that this has yet to be achieved but communicates the value of continued exploration of the electrostatic rotating machine multiplicative gain design space and the potential to develop "Moore's law" type trends. Tertiary attributes of electrostatic rotating machines that have only been discussed qualitatively also merit further study and include heat transfer/conduction using the dielectric fluid, additive manufacturing at scale, leveraging the incompressibility of a liquid-filled machine, and materials cost savings, among many other topics.

VIII. CONCLUSION

This article reviewed the macroscale electrostatic rotating machine landscape via published empirical data and analytical modeling to assess the state of the art and establish an innovation vector strategy for performance improvement. The empirical data revealed that electrostatic machines as a whole have lagged behind their magnetic counterparts at the macroscale by orders of magnitude but have enormous potential for performance improvement. In the past decade, there have been four orders of magnitude improvement in N·m/V^2, with work prior to that time remaining unchanged for nearly a century. At present, liquid-filled separately excited SEMs have demonstrated torque levels and torque densities similar to surface permanent magnet industrial servos but with the added advantage of minimal loss at low speeds and stall since the torque results from voltage. The rapid progress in electrostatic machines in recent years that closes the performance gap is due to a multiplicative gain design strategy, rather than any singular innovation. A multiphysics approach spanning dielectric liquids, cascaded stator–rotor axial gap maintenance, and advanced manufacturing (PCBs and 3-D printing) along with a three-phase separately excited machine topology driven by wide-bandgap medium-voltage power electronics make macroscale electrostatic rotating machines possible.

APPENDIX

See Tables II–V.

ACKNOWLEDGMENT

Daniel C. Ludois, Baoyun Ge, Aditya N. Ghule, and Ryan Knippel have ownership in C-Motive Technologies, a company commercializing electrostatic machines. The authors thank the Wisconsin Electric Machines and Power Electronics Consortium and its sponsors for their continued support.

REFERENCES

[1] O. Jefimenko, *Electrostatic Motors: Their History, Types and Principles of Operation*. Beltsville, MD, USA: Integrity Research Institute, 2011.
[2] D. Griffiths, *Introduction to Electrodynamics*, 3rd ed. Upper Saddle River, NJ, USA: Prentice-Hall, 1999.
[3] F. P. Grosu, M. K. Bologa, O. V. Motorin, I. V. Kozhevnikov, and A. A. Polikarpov, "Physical peculiarities of corona-discharge motors," *Surf. Eng. Appl. Electrochem.*, vol. 54, no. 6, pp. 585–592, Nov. 2018.
[4] M. Hattori, K. Asano, and Y. Higashiyama, "The fundamental characteristics of a cylindrical corona motor with multi-blade electrodes," *J. Electrostatics*, vol. 27, no. 3, pp. 223–235, Mar. 1992.
[5] P. T. Krein, "Analysis of corona motors and micromotors by means of effective gap conductivity," *IEEE Trans. Ind. Appl.*, vol. 31, no. 4, pp. 752–760, Jul./Aug. 1995.
[6] P. T. Krein, "Nonideal effects in electrostatic induction motors," Ph.D. dissertation, Elect. Eng., Univ. Illinois Urbana-Champaign, Champaign, IL, USA, 1982.

[7] C. L. Strong, "The amateur scientist: Electrostatic motors are powered by the electric field of the Earth," *Sci. Amer.*, vol. 231, no. 4, pp. 126–134, Oct. 1974.

[8] *Benjamin Franklin's Electric Motor—Engineering and Technology History Wiki*. Accessed: Mar. 25, 2020. [Online]. Available: https://ethw.org/Benjamin_Franklin%27s_Electric_Motor

[9] R. M. Walmsley, *Electricity in the Service of Man*. London, U.K.: Cassell Company, Ltd, 1911.

[10] B. Ge, "The modeling, design and demonstration of electrostatic synchronous machines," Ph.D. dissertation, Elect. Comput. Eng., Univ. Wisconsin-Madison, Madison, WI, USA, 2018.

[11] A. N. Ghule, "Torque modulation and self-sensing for separately excited synchronous electrostatic machines," Ph.D. dissertation, Elect. Comput. Eng., Univ. Wisconsin-Madison, Madison, WI, USA, 2019.

[12] O. Heaviside, *Electrical Papers*. Cambridge, U.K.: Cambridge Univ. Press, 1892.

[13] G. Reitz, B. Butrymowicz, J. Reed, B. Ge, and D. C. Ludois, "A switched elastance electrostatic machine constructed from sustainable elements for rotational actuators," in *Proc. IEEE Energy Convers. Congr. Expo. (ECCE)*, Oct. 2017, pp. 2389–2395.

[14] J. G. Trump, "Vacuum electrostatic engineering," Ph.D. dissertation, Elect. Eng., Massachusetts Inst. Technol., Cambridge, MA, USA, 1933.

[15] N. J. Felici, "Ten years of research on electrostatics at the University of Grenoble 1942-1952," *Brit. J. Appl. Phys.*, vol. 4, p. 62, Jan. 1953.

[16] R. O'Donnell, N. Schofield, A. C. Smith, and J. Cullen, "Design concepts for high-voltage variable-capacitance DC generators," *IEEE Trans. Ind. Appl.*, vol. 45, no. 5, pp. 1778–1784, Sep. 2009.

[17] B. Bollée, "Electrostatic motors," *Philips Tech. Rev.*, vol. 30, no. 6, pp. 178–194, 1969.

[18] D. W. Novotny, T. A. Lipo, and T. M. Jahns, "Introduction to electric machines and drives," Wisconsin Power Electron. Res. Center, Univ. Wisconsin, Madison, WI, USA, 2010.

[19] T. Sashida, "Electrostatic motor," U.S. Patent US 8 278 797 B2, Jun. 7, 2006.

[20] *Shinsei High Power Electrostatic Motor*. Accessed: 2007. [Online]. Available: http://www.shinsei-motor.com/English/techno/

[21] N. J. Felici, "Machines électrostatiques puissantes," *J. de Phys. et le Radium*, vol. 10, no. 4, pp. 137–144, 1949.

[22] J. W. Felici, "Electrostatic generators," *Electron. Power*, vol. 11, no. 5, pp. 169–171, May 1965.

[23] B. Ge, A. N. Ghule, and D. C. Ludois, "High torque density macroscale electrostatic rotating machines: Electrical design, generalized $d-q$ framework, and demonstration," *IEEE Trans. Ind. Appl.*, vol. 55, no. 2, pp. 1225–1238, Mar. 2019.

[24] S. F. Nagle, C. Livermore, L. G. Frechette, R. Ghodssi, and J. H. Lang, "An electric induction micromotor," *J. Microelectromech. Syst.*, vol. 14, no. 5, pp. 1127–1143, Oct. 2005.

[25] R. A. Vanslette, "Torque generation using ferroelectric materials," *IEEE Trans. Aerosp. Electron. Syst.*, vol. AES-1, no. 2, pp. 124–128, Oct. 1965.

[26] N. Tesla, *The Inventions, Researches and Writings of Nikola Tesla*. New York, NY, USA: Barnes & Noble, 2014.

[27] S. F. Philp, "The prospects for vacuum-insulated electric machines in the generation of HVDC power," in *Proc. IEEE Int. Conf. Electr. Insul.*, Jun. 1976, pp. 80–87.

[28] S. Philp, "The vacuum-insulated, varying-capacitance machine," *IEEE Trans. Electr. Insul.*, vol. EI-12, no. 2, pp. 130–136, Apr. 1977.

[29] W. R. Corliss, *Propulsion Systems for Space Flight*. New York, NY, USA: McGraw-Hill Book Company, Inc., 1960.

[30] J. R. Melcher, *Continuum Electromechanics*, 1st ed. Cambridge, MA, USA: MIT Press, 1981.

[31] S. Dal Choi and D. A. Dunn, "A surface-charge induction motor," *Proc. IEEE*, vol. 59, no. 5, pp. 737–748, May 1971.

[32] F. J. Santana, J. M. Monzon, S. Garcia-Alonso, and J. A. Montiel-Nelson, "Lumped parametric model for an electrostatic induction micromotor using GA," in *Proc. 35th Annu. Conf. IEEE Ind. Electron.*, Nov. 2009, pp. 4029–4033.

[33] W. S. N. Trimmer and K. J. Gabriel, "Design considerations for a practical electrostatic micro-motor," *Sens. Actuators*, vol. 11, no. 2, pp. 189–206, Mar. 1987.

[34] S. F. Bart and J. H. Lang, "Electroquasistatic induction micromotors," in *Proc. IEEE Micro Electro Mech. Syst., Invest. Micro Struct., Sensors, Actuat., Mach. Robots*, Feb. 1989, pp. 7–12.

[35] L. G. Frechette, S. F. Nagle, R. Ghodssi, S. D. Umans, M. A. Schmidt, and J. H. Lang, "An electrostatic induction micromotor supported on gas-lubricated bearings," in *Proc. 14th IEEE Int. Conf. Micro Electro Mech. Syst.*, Jan. 2001, pp. 290–293.

[36] S. F. Bart, T. A. Lober, R. T. Howe, J. H. Lang, and M. F. Schlecht, "Design considerations for micromachined electric actuators," *Sens. Actuators*, vol. 14, no. 3, pp. 269–292, Jul. 1988.

[37] T. C. Neugebauer, D. J. Perreault, J. H. Lang, and C. Livermore, "A six-phase multilevel inverter for MEMS electrostatic induction micromotors," *IEEE Trans. Circuits Syst. II, Exp. Briefs*, vol. 51, no. 2, pp. 49–56, Feb. 2004.

[38] B. Ge and D. C. Ludois, "Design concepts for a fluid-filled three-phase axial-peg-style electrostatic rotating machine utilizing variable elastance," *IEEE Trans. Ind. Appl.*, vol. 52, no. 3, pp. 2156–2166, May 2016.

[39] B. Ge and D. C. Ludois, "Dielectric liquids for enhanced field force in macro scale direct drive electrostatic actuators and rotating machinery," *IEEE Trans. Dielectr. Electr. Insul.*, vol. 23, no. 4, pp. 1924–1934, Aug. 2016.

[40] H. Polinder, F. F. A. Van Der Pijl, G.-J. De Vilder, and P. J. Tavner, "Comparison of direct-drive and geared generator concepts for wind turbines," *IEEE Trans. Energy Convers.*, vol. 21, no. 3, pp. 725–733, Sep. 2006.

[41] T. A. Lipo and W. Liu, "Comparison of AC motors to an ideal machine part I-conventional AC machines," in *Proc. IEEE Energy Convers. Congr. Expo. (ECCE)*, Sep. 2018, pp. 1581–1588.

[42] T. A. Lipo, W. Liu, and Z. Du, "Comparison of AC motors to an ideal machine part II-non-sinusoidal AC machines," in *Proc. IEEE Int. Electr. Mach. Drives Conf. (IEMDC)*, May 2019, pp. 1810–1817.

[43] W. B. Esson, "Notes on the design of multipolar dynamos," *J. Inst. Electr. Eng.*, vol. 20, no. 93, pp. 265–289, May 1891.

[44] E. Fukada, "History and recent progress in piezoelectric polymers," *IEEE Trans. Ultrason., Ferroelectr., Freq. Control*, vol. 47, no. 6, pp. 1277–1290, Nov. 2000.

[45] B. Gross, "Electret research–stages in its development," *IEEE Trans. Electr. Insul.*, vol. EI-21, no. 3, pp. 249–269, Jun. 1986.

[46] R. Gerhard-Multhaupt, "Electrets: Dielectrics with quasi-permanent charge or polarization," *IEEE Trans. Electr. Insul.*, vol. EI-22, no. 5, pp. 531–554, Oct. 1987.

[47] J. K. Noland, S. Nuzzo, A. Tessarolo, and E. F. Alves, "Excitation system technologies for wound-field synchronous machines: Survey of solutions and evolving trends," *IEEE Access*, vol. 7, pp. 109699–109718, 2019.

[48] F. J. Santana-Martin, J. M. Monzon-Verona, S. Garcia-Alonso, and J. A. Montiel-Nelson, "Analysis of spatial harmonics in a polyphase electrostatic induction micromotor," in *Proc. 19th Int. Conf. Electr. Mach. (ICEM)*, Sep. 2010, pp. 1–6.

[49] B. Ge, A. N. Ghule, and D. C. Ludois, "Three-dimensional printed fluid-filled electrostatic rotating machine designed with conformal mapping methods," *IEEE Trans. Ind. Appl.*, vol. 53, no. 5, pp. 4348–4359, Sep. 2017.

[50] T. B. Johansson, M. Van Dessel, R. Belmans, and W. Geysen, "Technique for finding the optimum geometry of electrostatic micromotors," *IEEE Trans. Ind. Appl.*, vol. 30, no. 4, pp. 912–919, Jul./Aug. 1994.

[51] D. Sequeira, K. Coonley, and B. Mann, "Topological optimization of variable area plate capacitors for coupled electromechanical energy harvesters," *J. Intell. Mater. Syst. Struct.*, vol. 30, no. 15, pp. 2198–2211, Sep. 2019.

[52] M. A. Lieberman and A. J. Lichtenberg, *Principles of Plasma Discharges and Materials Processing*, 2nd ed. Hoboken, NJ, USA: Wiley, 2005.

[53] W. W. Buechner, R. J. Van De Graaff, A. Sperduto, E. A. Burrill, L. R. Mcintosh, and R. C. Urquhart, "Electrostatic generator using sulphur hexafluoride insulation," *Phys. Rev.*, vol. 69, p. 692, Jun. 1946.

[54] J. G. Trump, F. J. Safford, and R. W. Cloud, "D-C breakdown strength of air and of freon in a uniform field at high pressures," *Trans. Amer. Inst. Electr. Eng.*, vol. 60, no. 3, pp. 132–135, Mar. 1941.

[55] R. L. Fortescue and P. D. Hall, "The high-voltage electrostatic generator at the atomic energy research establishment," *Proc. IEE I, Gen.*, vol. 96, no. 98, pp. 77–85, Mar. 1949.

[56] W. C. Johnson, "Axially gapped electrostatic machine having drive structure configured to recycle charge," U.S. Patent 10 056 848, May 4, 2013.

[57] W. M. Haynes, *CRC Handbook of Chemistry and Physics*, 93rd ed. Boca Raton, FL, USA: CRC Press, 2012.

[58] R. Ferguson, A. Lobeiras, and J. Sabou, "Suspended particles in the liquid insulation of aging power transformers," *IEEE Elect. Insul. Mag.*, vol. 18, no. 4, pp. 17–23, Jul. 2002.

[59] Z. Zhou, F. Bing, W. Tao, and X. Song, "Alternative method for the determination of the antioxidant content in transformer oil by electrochemical techniques," *IEEE Trans. Dielectr. Electr. Insul.*, vol. 19, no. 5, pp. 1498–1501, Oct. 2012.

[60] M. Zahn, "Space charge dynamics of liquids," Ph.D. dissertation, Elect. Eng., Massachusetts Inst. Technol., Cambridge, MA, USA, 1970.

[61] N. Felici, "High-field conduction in dielectric liquids revisited," *IEEE Trans. Electr. Insul.*, vol. EI-20, no. 2, pp. 233–238, Apr. 1985.

[62] T. Niino, T. Higuchi, and S. Egawa, "Dual excitation multiphase electrostatic drive," in *Proc. Conf. Rec. IEEE Ind. Appl. Conf. 13th IAS Annu. Meeting*, vol. 2, Oct. 1995, pp. 1318–1325.

[63] T. Niino, T. Higuchi, and S. Egawa, "AC dual excitation multiphase electrostatic drive," *J. Robot. Soc. Jpn.*, vol. 15, no. 1, pp. 97–102, 1997.

[64] B. Ge and D. C. Ludois, "Evaluation of dielectric fluids for macro-scale electrostatic actuators and machinery," in *Proc. IEEE Energy Convers. Congr. Expo. (ECCE)*, Sep. 2014, pp. 1457–1464.

[65] B. Ge and D. C. Ludois, "A 1-phase 48-pole axial peg style electrostatic rotating machine utilizing variable elastance," in *Proc. IEEE Int. Electr. Mach. Drives Conf. (IEMDC)*, May 2015, pp. 604–610.

[66] B. Ge and D. C. Ludois, "Design concepts for a 3-phase axial peg style electrostatic rotating machine utilizing variable elastance," in *Proc. IEEE Energy Convers. Congr. Expo. (ECCE)*, Sep. 2015, pp. 6519–6528.

[67] B. Ge, D. C. Ludois, and A. N. Ghule, "A 3D printed fluid filled variable elastance electrostatic machine optimized with conformal mapping," in *Proc. IEEE Energy Convers. Congr. Expo. (ECCE)*, Sep. 2016, pp. 1–8.

[68] K. J. Frankforter, D. J. Klingenberg, and D. C. Ludois, "Dielectric nanofluids for electrostatic machines & actuators," in *Proc. IEEE Ind. Appl. Soc. Annu. Meeting*, Sep. 2019, pp. 1–8.

[69] M. Dadkhah, Y. Hojjat, J. U. Jeon, M. Ghodsi, and M. Modabberifar, "Voltage-induction synchronous electrostatic motor," *Int. J. Adv. Manuf. Technol.*, vol. 77, nos. 1–4, pp. 145–164, Mar. 2015.

[70] R. Albers, "Theoretical and experimental studies of electrostatic ac generators with liquid polar Dielectrics," Ph.D. dissertation, Mech. Eng., Tech. Univ. Munich, Munich, Germany, 2002.

[71] M. A. Petrowsky, M. J. Erickson, D. C. Ludois, W. Mason, and J. K. Reed, "Electrostatic machine system and method of operation," U.S. Patent 9 866 148, Jan. 9, 2018.

[72] W. Dittrich, H. Hill, and E. Kinzel "Method for preparing high-purity propylene carbonate and for simultaneously making passivated electrodes," U.S. Patent US5 437 775 A Jan. 8, 1995.

[73] E. Acome *et al.*, "Hydraulically amplified self-healing electrostatic actuators with muscle-like performance," *Science*, vol. 359, no. 6371, pp. 61–65, Jan. 2018.

[74] N. Kellaris, V. G. Venkata, G. M. Smith, S. K. Mitchell, and C. Keplinger, "Peano-HASEL actuators: Muscle-mimetic, electrohydraulic transducers that linearly contract on activation," *Sci. Robot.*, vol. 3, no. 14, Jan. 2018, Art. no. eaar3276.

[75] N. Kellaris, V. G. Venkata, P. Rothemund, and C. Keplinger, "An analytical model for the design of peano-HASEL actuators with drastically improved performance," *Extreme Mech. Lett.*, vol. 29, May 2019, Art. no. 100449.

[76] S. K. Mitchell *et al.*, "An easy-to-implement toolkit to create versatile and high-performance HASEL actuators for untethered soft robots," *Adv. Sci.*, vol. 6, Jun. 2019, Art. no. 1900178.

[77] P. Rothemund, N. Kellaris, and C. Keplinger, "How inhomogeneous zipping increases the force output of peano-HASEL actuators," *Extreme Mech. Lett.*, vol. 31, Sep. 2019, Art. no. 100542.

[78] X. Wang, S. K. Mitchell, E. H. Rumley, P. Rothemund, and C. Keplinger, "High-strain Peano–HASEL actuators," *Adv. Funct. Mater.*, vol. 30, no. 7, 2020, Art. no. 1908821.

[79] S. S. Panwar, U. Gandhi, E. Acome, C. Keplinger, and M. Rowe, "Simulation-driven design to reduce pull-in voltage of donut HASEL actuators," in *Proc. Electroactive Polym. Actuat. Devices (EAPAD)*, Mar. 2019, Art. no. 1096622.

[80] C. Schunk *et al.*, "System identification and closed-loop control of a hydraulically amplified self-healing electrostatic (HASEL) actuator," in *Proc. IEEE/RSJ Int. Conf. Intell. Robots Syst. (IROS)*, Oct. 2018, pp. 6417–6423.

[81] P. Rumpelt and F. Jenau, "Oil impregnated pressboard barrier systems based on ester fluids for an application in HVDC insulation systems," *Energies*, vol. 10, no. 12, p. 2147, Dec. 2017.

[82] T. Park and Y. Cha, "Soft gripper actuated by electro-hydraulic force," *Proc. SPIE*, vol. 10966, Mar. 2019, Art. no. 109661Q.

[83] P.-W. Lin and C.-H. Liu, "Bio-inspired soft proboscis actuator driven by dielectric elastomer fluid transducers," *Polymers*, vol. 11, no. 1, p. 142, Jan. 2019.

[84] M. Duranti, M. Righi, R. Vertechy, and M. Fontana, "A new class of variable capacitance generators based on the dielectric fluid transducer," *Smart Mater. Struct.*, vol. 26, no. 11, Nov. 2017, Art. no. 115014.

[85] I.-D. Sirbu *et al.*, "Electrostatic actuator for tactile display based on hydraulically coupled dielectric fluids and soft structures," in *Proc. Electroactive Polym. Actuat. Devices (EAPAD)*, Mar. 2019, Art. no. 109662.

[86] T. G. Morrissey, S. K. Mitchell, A. T. Jaros, E. Ambos, and C. Keplinger, "Mechanical-to-electrical energy conversion with variable electric double layers," *Energy Technol.*, vol. 7, no. 4, Apr. 2019, Art. no. 1801007.

[87] J. K. Moon, J. Jeong, D. Lee, and H. K. Pak, "Electrical power generation by mechanically modulating electrical double layers," *Nature Commun.*, vol. 4, no. 1, pp. 1–6, Feb. 2013.

[88] D. C. Ludois and K. J. Frankforter, "A rotating double layer capacitive slip ring concept for power & heat transfer in machines using an ionic conducting working fluid," in *Proc. IEEE Energy Convers. Congr. Expo. (ECCE)*, Detroit, MI, USA, Oct. 2020.

[89] M. A. White, "Sustainable approaches to advanced materials research," *Phys. Canada*, vol. 68, no. 1, pp. 27–29, 2012.

[90] J. Dai and D. C. Ludois, "A survey of wireless power transfer and a critical comparison of inductive and capacitive coupling for small gap applications," *IEEE Trans. Power Electron.*, vol. 30, no. 11, pp. 6017–6029, Nov. 2015.

[91] R. P. Knippel, "Rotating capacitors with spiral groove features for hydrodynamic gap maintenance in power conversion systems," Ph.D. dissertation, Dept. Eng. Mech., Univ. Wisconsin-Madison, Madison, WI, USA, 2019.

[92] *Rolling Bearings and Seals in Electric Motors and Generators, Product Catalog PUB 54/P7 13459 EN*, SKF, Gothenburg, Sweden, Aug. 2013.

[93] R. Hoppler and R. A. Errath, "Motor bearings: 'The bearing necessities,'" ABB, Global Cement Mag., Baden, Switzerland, Tech. Rep., Oct. 2007. [Online]. Available: https://library.e.abb.com/public/63851c12adb74ab9c1257b350030730e/Motor%20bearings_reprint%20from%20Global%20Cement%20Magazine_3BHS%20260%20042%20ZAB%20E01.pdf

[94] Y. Hojjat, M. Dadkhah, M. Modabberifar, and M. Ghanbari, "Electrostatic rotation of plexiglas disc supported on air bearing," in *Proc. 14th Int. Conf. Mechatronics Mach. Vis. Pract.*, Dec. 2007, pp. 130–135.

[95] D. C. Ludois, M. J. Erickson, and J. K. Reed, "Aerodynamic fluid bearings for translational and rotating capacitors in noncontact capacitive power transfer systems," *IEEE Trans. Ind. Appl.*, vol. 50, no. 2, pp. 1025–1033, Mar. 2014.

[96] J.-B. Huanga, P.-S. Mao, and Q.-Y. Tong, "Study on Si electrostatic and electroquasistatic micromotors," *Sens. Actuators A, Phys.*, vol. 35, no. 3, pp. 171–174, Feb. 1993.

[97] R. Knippel, M. Tisler, and D. C. Ludois, "Printed circuit board structural properties and spiral groove trace conductors for hydrodynamic gap maintenance in axial flux rotating machines," in *Proc. IEEE Energy Convers. Congr. Expo. (ECCE)*, Sep. 2019, pp. 6084–6091.

[98] R. F. Post, "Electrostatic generator/motor configurations," U.S. Patent 8 643 249 B2, Sep. 10, 2007.

[99] S. F. Nagel, "Analysis, design, and fabrication of an electrostatic induction micromotor for a micro gas-turbine generator," Ph.D. dissertation, Elect. Eng., Massachusetts Inst. Technol., Cambridge, MA, USA, 2000.

[100] L. G. Frechette, "Development of a microfabricated silicon motor-driven compressor system," Ph.D. dissertation, Dept. Aeronaut. Astronaut., Massachusetts Inst. Technol., Cambridge, MA, USA, 2000.

[101] D. C. Ludois, J. Reed, and M. Erickson, "Aerodynamic fluid bearings for capacitive power transfer and rotating machinery," in *Proc. IEEE Energy Convers. Congr. Expo. (ECCE)*, Sep. 2012, pp. 1932–1937.

[102] A. Di Gioia *et al.*, "Design and demonstration of a wound field synchronous machine for electric vehicle traction with brushless capacitive field excitation," *IEEE Trans. Ind. Appl.*, vol. 54, no. 2, pp. 1390–1403, Mar. 2018.

[103] J. Dai, S. Hagen, D. C. Ludois, and I. P. Brown, "Synchronous generator brushless field excitation and voltage regulation via capacitive coupling through journal bearings," *IEEE Trans. Ind. Appl.*, vol. 53, no. 4, pp. 3317–3326, Jul. 2017.

[104] S. Hagen, R. Knippel, J. Dai, and D. C. Ludois, "Capacitive coupling through a hydrodynamic journal bearing to power rotating electrical loads without contact," in *Proc. IEEE Wireless Power Transf. Conf. (WPTC)*, May 2015, pp. 1–4.

[105] E. A. Muijderman, "Analysis and design of spiral-groove bearings," *J. Lubrication Technol.*, vol. 89, no. 3, pp. 291–305, Jul. 1967.

[106] D. C. Ludois, "Varying capacitance rotating electrical machine," U.S. Patent 9 184 676 B2, Nov. 10, 2015.

[107] D. C. Ludois and M. J. Erickson, "Self-conforming plates for capacitive machines such as electrostatic motors and generators," U.S. Patent 9 479 085, Oct. 25, 2016.

[108] J. E. Colgate, H. Matsumoto, and W. Wannasuphoprasit, "Linear electrostatic actuators: Gap maintenance via fluid bearings," *Robot. Comput.-Integr. Manuf.*, vol. 10, no. 5, pp. 365–376, Oct. 1993.

[109] F. T. Han, L. Wang, Q. P. Wu, and Y. F. Liu, "Performance of an active electric bearing for rotary micromotors," *J. Micromech. Microeng.*, vol. 21, no. 8, Jul. 2011, Art. no. 085027.

[110] S. Kumar, D. Cho, and W. Carr, "Electric levitation bearings for micromotors," in *IEEE Int. Solid-State Circuits Conf. (ISSCC) Dig. Tech. Papers*, Jun. 1991, pp. 882–885.

[111] G. He, K. Chen, S. Tan, and W. Wang, "Electrical levitation for micromotors, microgyroscopes and microaccelerometers," *Sens. Actuators A, Phys.*, vol. 54, nos. 1–3, pp. 741–745, Jun. 1996.

[112] L. Jin, T. Higuchi, and M. Kanemoto, "Electrostatic levitator for hard disk media," *IEEE Trans. Ind. Electron.*, vol. 42, no. 5, pp. 467–473, Oct. 1995.

[113] E. van West, A. Yamamoto, and T. Higuchi, "Pick and place of hard disk media using electrostatic levitation," in *Proc. IEEE Int. Conf. Robot. Autom.*, Apr. 2007, pp. 2520–2525.

[114] T. Higuchi, "Clean and non-contact transportation Technology. Electrostatic suspension and propulsion of silicon wafer and glass plate," *J. Jpn. Soc. Precis. Eng.*, vol. 63, no. 7, pp. 943–946, 1997.

[115] D. Ludois and E. Severson, "Bearing-less electrostatic flywheel," U.S. Patent 20 200 036 299, Jul. 24, 2018.

[116] M. Mayberry, D. C. Ludois, and E. Severson, "Towards electrostatic levitation of rotating machines," in *Proc. IEEE Energy Convers. Congr. Expo. (ECCE)*, Detroit, MI, USA, Oct. 2020.

[117] N. Zhao *et al.*, "Development of a dielectric-gas-based single-phase electrostatic motor," *IEEE Trans. Ind. Appl.*, vol. 55, no. 3, pp. 2592–2600, May 2019.

[118] B. Ge, A. N. Ghule, and D. C. Ludois, "A dq-axis framework for electrostatic synchronous machines and charge oriented control," in *Proc. IEEE Energy Convers. Congr. Expo. (ECCE)*, Oct. 2017, pp. 2396–2403.

[119] F. Kimura, A. Yamamoto, and T. Higuchi, "FPGA implementation of a signal synthesizer for driving a high-power electrostatic motor," in *Proc. IEEE Int. Symp. Ind. Electron.*, Jun. 2011, pp. 1295–1300.

[120] A. N. Ghule, P. Killeen, and D. C. Ludois, "Synchronous electrostatic machine torque modulation via complex vector voltage control with a current source inverter," *IEEE J. Emerg. Sel. Topics Power Electron.*, vol. 8, no. 2, pp. 1850–1857, Jun. 2020.

[121] A. N. Ghule, B. Ge, and D. C. Ludois, "Variable frequency electrostatic drive," U.S. Patent 960 719, May 1, 2018.

[122] S. Kim and S. K. Sul, "Sensorless control of AC motor—Where are we now?" in *Proc. Int. Conf. Electr. Mach. Syst. (ICEMS)*, Aug. 2011, pp. 1–6.

[123] A. N. Ghule, P. Killeen, and D. C. Ludois, "High frequency injection based rotor position self-sensing for synchronous electrostatic machines," in *Proc. IEEE Energy Convers. Congr. Expo. (ECCE)*, Sep. 2019, pp. 804–811.

[124] S. Kouro *et al.*, "Recent advances and industrial applications of multilevel converters," *IEEE Trans. Ind. Electron.*, vol. 57, no. 8, pp. 2553–2580, Aug. 2010.

[125] M. A. Perez, S. Bernet, J. Rodriguez, S. Kouro, and R. Lizana, "Circuit topologies, modeling, control schemes, and applications of modular multilevel converters," *IEEE Trans. Power Electron.*, vol. 30, no. 1, pp. 4–17, Jan. 2015.

[126] V. Veliadis. (2019). *PowerAmerica Manufacturing Institute*. Accessed: Jan. 2, 2020. [Online]. Available: https://www.energy.gov/sites/prod/files/2019/07/f64/006-Consortia19-PowerAmericaInstitute.pdf

[127] V. Pala *et al.*, "10 kV and 15 kV silicon carbide power MOSFETs for next-generation energy conversion and transmission systems," in *Proc. IEEE Energy Convers. Congr. Expo. (ECCE)*, Sep. 2014, pp. 449–454.

[128] C. DiMarino, I. Cvetkovic, Z. Shen, R. Burgos, and D. Boroyevich, "10 kV, 120 a SiC MOSFET modules for a power electronics building block (PEBB)," in *Proc. IEEE Workshop Wide Bandgap Power Devices Appl.*, Oct. 2014, pp. 55–58.

[129] M. K. Das *et al.*, "10 kV, 120 a SiC half H-bridge power MOSFET modules suitable for high frequency, medium voltage applications," in *Proc. IEEE Energy Convers. Congr. Expo.*, Sep. 2011, pp. 2689–2692.

[130] B. Passmore *et al.*, "The next generation of high voltage (10 kV) silicon carbide power modules," in *Proc. IEEE 4th Workshop Wide Bandgap Power Devices Appl. (WiPDA)*, Nov. 2016, pp. 1–4.

[131] P. Killeen, A. N. Ghule, and D. C. Ludois, "Silicon carbide JFET super-cascodes for normally-on current source inverter switches in medium voltage variable speed electrostatic drives," in *Proc. IEEE Energy Convers. Congr. Expo. (ECCE)*, Sep. 2019, pp. 4004–4011.

[132] P. Killeen and D. C. Ludois, "Evaluation of drive topologies for macro scale synchronous electrostatic machines," in *Proc. 22nd Eur. Conf. Power Electron. Appl.*, Lyon, France, Sep. 2020.

[133] P. Killeen and D. C. Ludois, "Three-phase bidirectional-flyback differential-inverter for synchronous electrostatic machines," in *Proc. IEEE Energy Convers. Congr. Expo. (ECCE)*, Detroit, MI, USA, Oct. 2020.

[134] E. R. Mognaschi and J. H. Calderwood, "Asynchronous dielectric induction motor," *IEE Proc. A (Phys. Sci., Meas. Instrum., Manage. Educ.)*, vol. 137, no. 6, pp. 331–338, Nov. 1990.

Daniel C. Ludois (Senior Member, IEEE) received the B.S. degree in physics from Bradley University, Peoria, IL, USA, in 2006, and the M.S. and Ph.D. degrees in electrical engineering at the University of Wisconsin–Madison (UW-Madison), Madison, WI, USA, in 2008 and 2012, respectively.

He cofounded C-Motive Technologies Inc., Madison, in 2012, a company developing capacitively coupled power conversion technologies. Today, C-Motive is working to commercialize electrostatic machines. In 2013, he joined the faculty of the Department of Electrical and Computer Engineering, UW-Madison, where he is currently a Jean van Bladel Associate Professor. He is also an Associate Director of the Wisconsin Electric Machines and Power Electronics Consortium (WEMPEC), UW-Madison. He has coauthored four IEEE prize papers. His research interests include power electronics, electric machines, applied electromagnetics, and entrepreneurship.

Dr. Ludois received the USA National Science Foundation CAREER Award in 2015 and was named a Moore Inventor Fellow by the Gordon & Betty Moore Foundation in 2017.

Kevin J. Frankforter (Member, IEEE) received the B.Sc. degree in electrical engineering from the University of Nebraska–Lincoln, Lincoln, NE, USA, in 2010, and the M.Sc. and Ph.D. degrees in electrical engineering from the University of Wisconsin–Madison, Madison, WI, USA, in 2014 and 2018, respectively.

He performed his graduate studies at the University of Wisconsin–Madison as a member of the Wisconsin Electric Machines and Power Electronics Consortium, where he was with the Environmental Chemistry and Technology Program. Since graduating, he has been a Post-Doctoral Research Associate with the University of Wisconsin–Madison. His research interests include power engineering, energy storage, and applied chemistry and materials science.

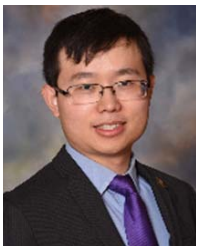

Baoyun Ge (Member, IEEE) received the B.S. degree in electrical engineering from Southeast University, Nanjing, China, in 2012, and the Ph.D. degree in electrical engineering from the Wisconsin Electric Machines and Power Electronics Consortium, University of Wisconsin–Madison, Madison, WI, USA, in 2018.

He is currently with C-Motive Technologies Inc., Madison, a startup company developing capacitively coupled power conversion technologies. His research interests include electric machines, power electronics, and high-performance electromagnetic computation.

Dr. Ge received the First Place Paper Award and the Third Place Thesis Award from the IEEE Industry Application Society (IAS) in 2017 and 2019, respectively.

Aditya N. Ghule (Member, IEEE) received the B.Tech. degree in electrical engineering from the College of Engineering Pune, Pune, India, in 2010, and the M.S. degrees in electrical engineering and mechanical engineering and the Ph.D. degree in electrical engineering from the University of Wisconsin-Madison, Madison, WI, USA, in 2013 and 2019, respectively.

Between his graduate degree pursuits, he was with Unico Inc., Franksville, WI, USA, from 2013 to 2016, working in drive systems development. He is currently with C-Motive Technologies, Inc., Madison, WI, USA. His research interests include the control of electric machines and power electronics.

Peter Killeen (Student Member, IEEE) received the B.S. degree in electrical engineering from the University of Arkansas, Fayetteville, AR, USA, in 2012. He is currently pursuing the Ph.D. degree with the University of Wisconsin–Madison, Madison, WI, USA.

From 2012 to 2016, he was with Wolfspeed, Fayetteville, working on wide bandgap power electronics. His research interests include power electronics and drives for electric machines.

Ryan Knippel (Member, IEEE) received the B.S., M.S., and Ph.D. degrees in engineering mechanics from the University of Wisconsin–Madison, Madison, WI, USA, in 2012, 2014, and 2019, respectively.

His Ph.D. research in engineering mechanics was through the Wisconsin Electric Machines and Power Electronics Consortium, University of Wisconsin–Madison. Since 2019, he has been with C-Motive Technologies Inc., Madison. His research interests focus on the mechanical and hydrodynamic design of rotating machines.